nature communications

Article

https://doi.org/10.1038/s41467-025-58289-1

Immunotherapy with conventional type-1 dendritic cells induces immune memory and limits tumor relapse

Received: 21 November 2023

Accepted: 17 March 2025

Published online: 09 April 2025

Check for updates

Ignacio Heras-Murillo[1], Diego Mañanes[1,2], Pablo Munné[1], Vanessa Núñez[1], Jessica Herrera[1], Mauro Catalá-Montoro[1], Maite Alvarez[3], Miguel A. del Pozo[1], Ignacio Melero[3,4,5,6], Stefanie K. Wculek[1,7,8] ✉ & David Sancho[1,8] ✉

The potential of dendritic cell (DC) vaccination against cancer is not fully achieved. Little is known about the precise nature of the anti-cancer immune response triggered by different natural DC subsets and their relevance in preventing postsurgical tumor recurrence. Here, we use mouse splenic conventional DC1s (cDC1s) or cDC2s pulsed with tumor cell lysates to generate DC vaccines. cDC1-based vaccination induces a stronger effector and memory $CD4^+$ and $CD8^+$ anti-tumor T cell response, leading to a better control of tumors treated either therapeutically or prophylactically. Using an experimental model of tumor relapse, we show that adjuvant or neoadjuvant cDC1 vaccination improves anti-tumor immune memory, particularly by increasing the infiltrates of $CD4^+$ tissue resident memory (Trm) and $CD8^+$ memory T cells. This translates into complete prevention of tumor relapses. Moreover, elevated abundance of cDC1s positively correlates with $CD4^+$ Trm presence, and both associate with enhanced survival in human breast cancer and melanoma. Our findings suggest that cDC1-based vaccination excels at immune memory induction and prevention of cancer recurrence.

The success of immune checkpoint blockade (ICB) highlights the potential of targeting the immune system to treat cancer. ICB is largely based on circumventing exhaustion of T cells to invigorate anti-cancer immunity[1]. However, a pressing clinical challenge is to prevent postsurgical cancer recurrence[2,3]. Promoting long-term local and systemic cancer immune surveillance represents a promising therapeutic approach to tackle this unmet medical need[4].

Natural immunity against tumors gives rise to circulating (effector memory and central memory) and resident memory (Trm) T cells, which differ in their migration pattern and function[5]. Increased presence of memory $CD8^+$ T cells in tumors correlates with improved outcomes for cancer patients[6,7]. Despite being less characterized, the potency of memory $CD4^+$ T cells for anti-cancer immunity is emerging[8], and circulating[9] as well as resident[10] memory $CD4^+$ T cells are associated with anti-tumor immunity. Pre-clinical evidence suggests that circulating and resident memory T cells cooperate to protect against tumor re-challenge[11–13]. Thus, strategies that induce both memory T cell subsets will represent future immunotherapies to prevent tumor recurrence.

Dendritic cells (DCs) are a functionally diverse group of professional antigen-presenting cells (APCs) that control adaptive immunity. Adoptive transfer of ex vivo activated and tumor antigen-loaded DCs (DC vaccination) induces cancer-controlling immune effector and memory responses in pre-clinical models[14,15]. However, the nature of

[1]Centro Nacional de Investigaciones Cardiovasculares (CNIC), Madrid, Spain. [2]Universidad Autónoma de Madrid, Escuela de Doctorado, Madrid, Spain. [3]Program of Immunology and Immunotherapy, CIMA Universidad de Navarra, Pamplona, Spain. [4]Navarra Institute for Health Research (IDISNA), Pamplona, Spain. [5]Centro de Investigación Biomédica en Red de Cáncer (CIBERONC), Madrid, Spain. [6]Nuffield Department of Medicine and Churchill Hospital. University of Oxford, Oxford, UK. [7]Institute for Research in Biomedicine (IRB Barcelona), The Barcelona Institute of Science and Technology (BIST), Barcelona, Spain. [8]These authors contributed equally: Stefanie K. Wculek, David Sancho. ✉e-mail: stefanie.wculek@irbbarcelona.org; dsancho@cnic.es

the T cell memory induced by tumor antigen-loaded DC treatment is largely elusive, particularly in settings where a natural anti-tumor immunity is present. In light of the ongoing clinical trials of adjuvant (after tumor surgery) DC vaccination in patients with cancer[16,17], it is of the upmost importance to assess the capacity of DC-based therapy to improve the naturally generated anti-cancer T cell memory in tumor-experienced hosts.

To this end, exploiting distinct DC subsets to induce optimal anti-cancer effector and memory T cell responses holds great potential. Naturally occurring conventional DCs (cDCs) are ontogenically and functionally subdivided into type 1 (cDC1) and 2 (cDC2) subsets and harbor the largest potential for T cell priming[18]. However, DC vaccination studies have mostly used DC surrogates generated from bone marrow (BMDCs) or blood monocytes (moDCs)[19,20]. These cells often do not directly present tumor antigen to T cells in vivo but require endogenous cDCs for therapeutic efficacy[21–23] and their anti-cancer potential is lower compared to cDCs[24]. This evidence led to the development of next-generation DC cancer vaccines based on autologous natural DCs. cDC1s excel at cross-presentation to activate anti-cancer $CD8^+$ T cells[25,26] and also contribute to anti-tumor $CD4^+$ T cell priming[27]. Furthermore, cDC1s are required for the efficacy of ICB[28–30], and their elevated intratumoral presence positively correlates with $CD8^+$ T cell abundance and favorable prognosis of cancer patients[31,32]. The pre-clinical effectiveness of transfer of in vitro-generated cDC1-like cells outperforms that of moDCs[33] and does not rely on host cDCs[24]. The efficacy of natural splenic cDC1-based vaccination to reduce cancer progression was demonstrated in pre-clinical models[14]. Moreover, the first phase I/II clinical trials administering cDC1s and cDC2s[34] or purified cDC1s (NCT05773859) show the feasibility and safety of cDC1 vaccination for cancer patients. cDC2s initiate $CD4^+$ T cell responses[35] and can cross-present and prime $CD8^+$ T cells in tumor contexts[36–39].While clinical trials treating prostate cancer and melanoma patients with circulating $CD1c^+$ cDC2s are showing promising antigen-specific responses that correlate with clinical outcome[17,40,41], a completed phase III clinical trial using adjuvant vaccination with cDC2s and pDCs in melanoma patients showed no benefit in survival[42]. Pre-clinical data using cDC2-like cells for anti-tumor vaccination are contradictory, which suggests context- and antigen-dependent functions of cDC2s[24,43]. Notably, apart from tumor-extracted cDCs[43], the efficacy of adoptive transfer of ex vivo tumor antigen-loaded natural cDC1s or cDC2s to promote anti-cancer effector or memory T cell responses has not been assessed in comparative studies.

Here, we optimized the preparation of syngeneic mouse spleen-derived cDC1s and cDC2s loaded with tumor lysates to induce anti-tumor $CD4^+$ and $CD8^+$ T cell responses upon administration to mice. cDC1-based vaccination was largely superior to cDC2-based treatments in inducing cancer-specific effector and memory T cells, and in reducing cancer progression in therapeutic and prophylactic approaches. Furthermore, administration of cDC1s in neoadjuvant and adjuvant settings prevented tumor recurrence in pre-clinical cancer surgery models, far beyond natural or ICB-induced cancer protection. Neoadjuvant cDC1-based therapy induced elevated numbers of $CD8^+$ T cells and, specifically, $CD4^+$ Trm cells in relapsing tumors just before their remission. Notably, increased $CD4^+$ Trm prevalence correlated with cDC1 presence in human tumors and patient survival. Hence, our results suggest that cDC1 vaccination triggers a qualitatively unique immune memory response that strongly protects from tumor recurrence.

Results

cDC1s are superior to cDC2-based cancer vaccination in generation of $CD4^+$ Th1 and $CD8^+$ T cell effector responses

The blood is the most feasible source of autologous cDCs in cancer patients[44]. Transcriptional comparative analyses established that mouse splenic $CD8^+$ cDC1s are the equivalents of human circulating $CD141^+$ cDC1s[45] and mouse splenic $CD11b^+$ cDC2s largely resemble human circulating $CD1c^+$ cDC2s[46]. Therefore, we studied the efficacy of mouse splenic cDCs as basis for pre-clinical cancer vaccines. Mice bearing a B16 melanoma expressing FMS-like tyrosine kinase 3 ligand (Flt3L), a cDC mobilizing factor[47], served as cDC sources to reproduce the context of a cancer patient and to expand cDCs. Splenic $CD8^+$ cDC1s remain largely unaltered in this setting[14]. Splenic cDC2s from B16-Flt3L tumor-bearing mice also resemble their naive counterparts with similar expression of the cDC2-associated molecules MHC-II, CD11c, and SIRPα as well as absence of the macrophage/moDC markers CCR2, Ly6C, MERTK, and CD115, despite minor upregulation of CD11b due to FLT3L-mediated mobilization (Supplementary Fig. 1).

To compare the efficacy of natural splenic cDC1s with cDC2s for anti-cancer immunotherapy, we optimized the duration of ex vivo antigen exposure and immunogenic stimulation separately. Tumor cell lysate (TCL) produced by UV light-induced immunogenic cell death (ICD) of cancer cells was used as tumor cell-associated antigen due to its immunostimulatory properties and universality[14]. For DC activation, we explored the following toll-like receptor (TLR) agonists: Poly(I:C) (PIC) for TLR3 (expressed preferentially by cDC1s); lipopolysaccharide-EK (LPS) for TLR4; R848 for TLR7/8 (highly expressed by cDC2s) and CpG-ODN1826 (CpG) for TLR9 (expressed similarly by both)[18]. Splenic cDC1s and cDC2s were incubated with TCL of B16 melanoma cells expressing ovalbumin (B16-OVA) and TLR agonists individually or in combination for 1, 4, or 16 h. Then, we assessed the potential of cDCs to induce de novo activation of MHC-I $OVA_{257–264}$ peptide-specific $CD8^+$ T cells (OT-I) and MHC-II $OVA_{323–339}$ peptide-specific $CD4^+$ T cells (OT-II) ex vivo (Fig. 1a). cDC1s most consistently promoted proliferation of OT-I cells after 1 h of TLR agonist/TCL incubation (Fig. 1b, left panels). 16 h TLR agonist/TCL incubation of cDC1s could not be tested due to their impaired viability. cDC2s induced the strongest activation of OVA-specific T cells after 4 h TLR agonist/TCL exposure (Fig. 1b, right panels). Hence, we established 1 h for cDC1s and 4 h for cDC2 as optimal TLR agonist/TCL incubation time to promote their capacity to activate T cells (Fig. 1c). Moreover, CpG resulted as effective as all four TLR agonists combined for the induction of T cell proliferation by cDC1s and cDC2s (Fig. 1b). The expression of the key activation markers *Ccr7* (receptor for migration), *Cd40* (co-stimulatory molecule), *Ifnb1* and *Il12b* (involved in T cell activation) by cDCs were analyzed to confirm the effect of TLR agonists. Combining diverse TLR agonists did not enhance the activation of cDCs compared with CpG alone, apart from the known PIC response gene *Ifnb1*[48] (Supplementary Fig. 2a).

Next, we analyzed the generation of $CD4^+$ and $CD8^+$ T cell effector responses from the endogenous repertoire by adoptively transferred splenic cDC1s and cDC2s in vivo. cDC1s and cDC2s were incubated with B16-OVA TCL and CpG or the combined four TLR agonists and intradermally transferred into naive mice (Fig. 1d). Activation of antigen-specific T cells was analyzed by re-stimulation of inguinal lymph node (iLN) cells with APCs that were preloaded with $OVA_{257–264}$ peptide, $OVA_{323–339}$ peptide or B16-OVA TCL. The number of antigen-specific activated IFNγ-producing $CD44^+$ $CD4^+$ or $CD8^+$ T cells was elevated in all mice that received cDCs compared to untreated control mice. Ex vivo incubation of cDC1s with TCL and CpG or all four TLR agonist combined equally increased the cellularity of iLNs and the number of $IFNγ^+$ $CD44^+$ $CD4^+$ or $CD8^+$ T cells in treated mice. Of note, the capacity of cDC1s to prime OVA-specific $CD4^+$ T cells from the endogenous repertoire is superior compared with the limited priming of OT-II cells, consistent with previous reports[35]. The potency of cDC2s for T cell activation was not further enhanced upon incubation with TLR agonists together with TCL (Fig. 1e, f, and Supplementary Fig. 2b). This indicates the immune-stimulatory properties of ICD-induced TCL, which contains the TLR4 ligand high-mobility group box protein 1 (HMGB1)[14]. Of note, activation of cDC1s and cDC2s for T cell priming with CpG was not further improved when additionally adding LPS + PIC + R848 (Fig. 1 and Supplementary Fig. 2). Therefore, CpG alone was chosen as the cDC activation-inducing agent for all subsequent

https://doi.org/10.1038/s41467-025-58289-1

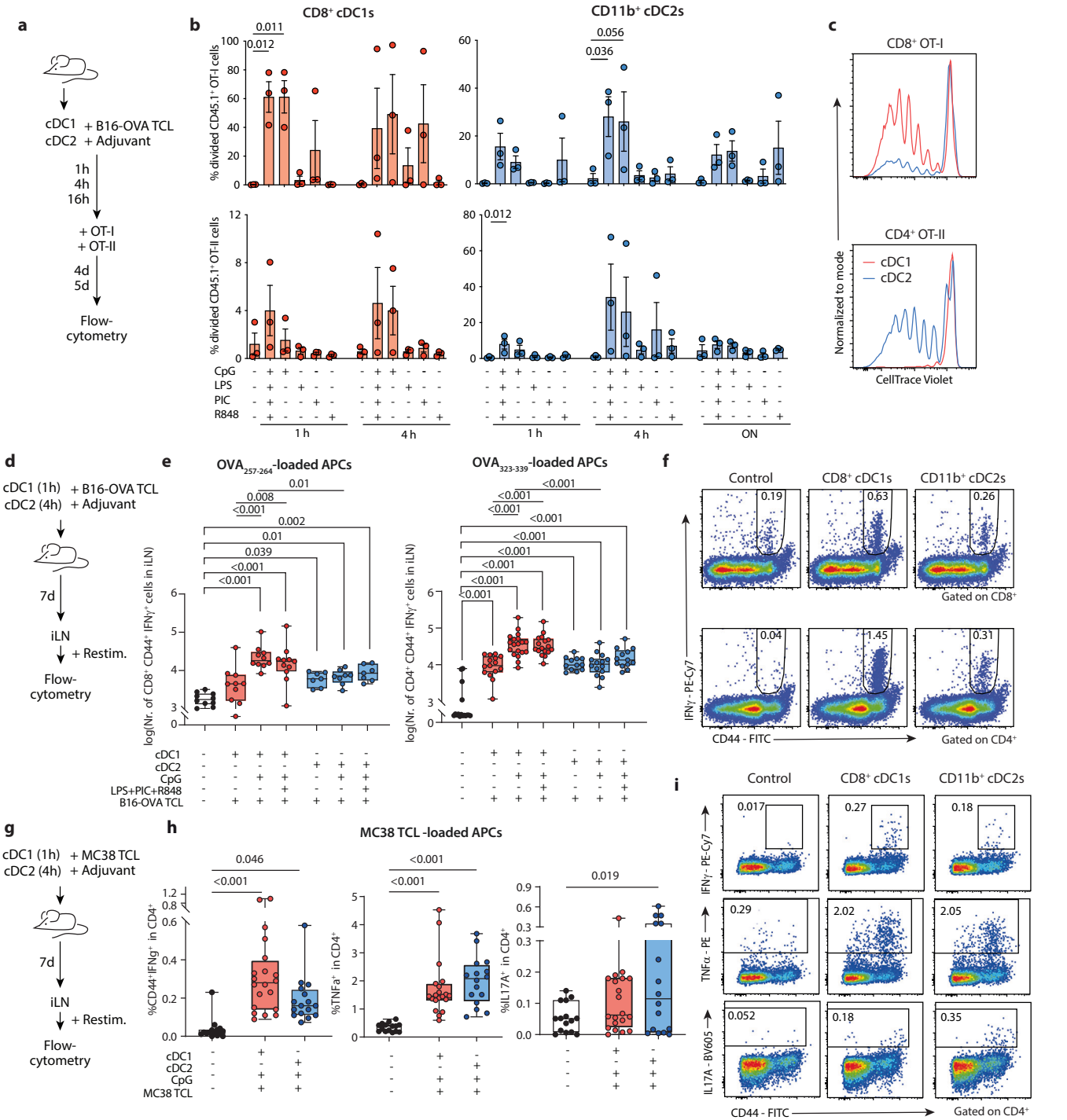

Fig. 1 | Transfer of activated and tumor antigen-loaded splenic cDC1s outperforms cDC2s in inducing a cancer-specific CD4⁺ Th1 and CD8⁺ T cell effector response. a Experimental overview for **b-c**: splenic cDC1s and cDC2s were incubated with B16-OVA TCL and TLR agonists for 1, 4, and 16 h (overnight, ON) and co-cultured with cell trace violet (CTV)-labeled naive OT-I or OT-II cells. **b** Flow cytometric analysis of frequency of divided OT-I and OT-II cells ($n = 3$ biological replicates/group from 3 independent experiments). **c** Representative histograms depicting CTV dilution for OT-I and OT-II co-cultured with 1 h (cDC1s) or 4 h (cDC2s) TCL+CpG-pulsed cDCs. **d** Experimental overview for (**e**, **f**): B16-OVA TCL + TLR agonist-treated cDC1s (1 h) and cDC2s (4 h) were injected intradermally in the flank of mice. Controls received PBS injection. IFNγ production by T cells in the iLN upon restimulation was assessed 7 days later. **e** Log-transformed number of activated CD44⁺ IFNγ⁺ CD8⁺ or CD4⁺ T cells in iLN (left to right: $n = 10, 10, 10, 11, 7, 8, 7$ [$OVA_{257-264}$]; 16, 15, 19, 17, 12, 14, 13 [$OVA_{323-339}$] biological replicates/group from 4 independent experiments). **f** Representative dot plots of CD8⁺ and CD4⁺ T cells from the iLN of mice untreated or treated with TCL+CpG-incubated cDC1s or cDC2s. **g** Experimental overview for (**h**, **i**): MC38 TCL+CpG-pulsed cDC1s (1 h) and cDC2s (4 h) were injected intradermally in the flank of mice. Controls received PBS injection. 7 days later, the IFNγ, TNFα, and IL17A production by CD4⁺ T cells in the iLN upon restimulation with MC38 TCL-loaded APCs was evaluated. **h**, Frequency of CD44⁺ IFNγ⁺, TNFα⁺, and IL17A⁺ in CD4⁺ T cells in iLN ($n = 15$ [PBS], 20 [cDC1], 16 [cDC2] biological replicates/group from 4 independent experiments). **i** Representative dot plots of CD4⁺ T cells of mice untreated or treated with CpG+TCL-incubated cDC1s or cDC2s. Data are presented as mean ± SEM (**b**) or box plots where whiskers represent minimum and maximum values, boxes indicate median, 25th, and 75th percentiles (**e**, **h**). Dots represent individual data points. Statistical analysis by paired (**b**) or unpaired (**e**, **h**) one-way ANOVA Tukey post-hoc test. Source data are provided as Source Data file.

https://doi.org/10.1038/s41467-025-58289-1

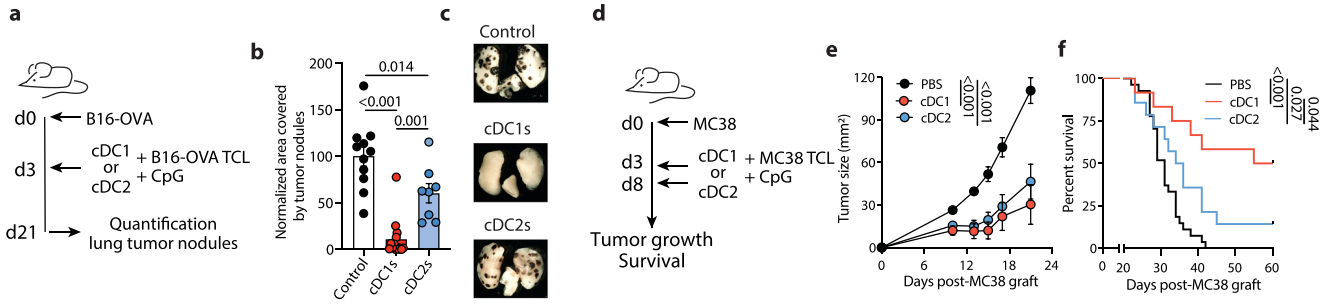

Fig. 2 | The therapeutic efficacy of cDC1-based anti-cancer vaccination is superior to cDC2s. a Experimental overview for (**b**, **c**): 4×10^5 B16-OVA cells were intravenously (i.v.) injected into naive mice. On day 3, the mice received an i.v. injection of 10^6 B16-OVA-TCL+CpG-pulsed splenic cDC1s or cDC2s or PBS as control. Lungs were harvested on day 21 for analysis. **b** Lung area covered by tumor nodules normalized to untreated control lungs is shown ($n = 12$ [control], 14 [cDC1], 8 [cDC2] biological replicates/group from 2 independent experiments). **c** Representative image of 3 lung lobes harboring tumor nodules. **d** Experimental overview for (**e**, **f**): 5×10^5 MC38 cells were subcutaneously (s.c.) injected in the right flank of naive mice. On day 3 and 8, the mice received intradermal (i.d.) injections of 10^6 MC38-TCL+CpG-pulsed splenic cDC1s or cDC2s or PBS (control). **e** Tumor growth and (**f**) humane endpoint are shown ($n = 27$ [control], 12 [cDC1], 14 [cDC2] biological replicates/group from 3 independent experiments). Data are presented as mean ± SEM (dots represent individual data points). Statistical analysis by one-way ANOVA and Tukey post-hoc test (**b**), two-way ANOVA (**e**) and Mantel-Cox test (**f**). Source data are provided as Source Data file.

experiments. Adoptive transfer of CpG-treated and TCL-loaded cDC1s and cDC2s did not enhance the presence of Foxp3$^+$ CD25$^+$ regulatory T cells (Tregs; Supplementary Fig. 2c, d).

Further, we examined T cell responses that were induced by cDC vaccines independent of exogenous model antigens. For that, cDC1 and cDC2 vaccines were prepared using TCL of the colon adenocarcinoma cell line MC38, activated with CpG and intradermally administered into naive mice. The resulting antigen-specific T cell effector response was analyzed by re-stimulation of the iLN with APCs preloaded with MC38 TCL, thus revealing MC38-specific T cell responses in an agnostic manner (Fig. 1g). The number of IFNγ-producing CD44$^+$ CD8$^+$ T cells was comparably elevated in cDC1 and cDC2-treated mice versus controls, demonstrating the generation of tumor-specific CD8$^+$ T cell activation in the absence of exogenous antigens (Supplementary Fig. 2e). The frequency of activated MC38 TCL-specific TNFα-producing CD4$^+$ T cells was also similarly increased upon treatment with either cDC vaccine. However, in line with previous reports[43], adoptive transfer of cDC2s induced IL17A-producing CD4$^+$ T cells, while cDC1s excelled at priming a tumor-specific CD4$^+$ Th1 effector response in vivo (Fig. 1h, i).

Overall, we defined ex vivo TCL+CpG treatment of splenic cDC1s for 1 h and cDC2s for 4 h as optimized T cell-stimulatory DC vaccine preparations. Additionally, we demonstrated that cDC1s generate superior tumor antigen-specific CD4$^+$ Th1 effector T cell responses from the endogenous repertoire upon adoptive transfer in vivo compared to cDC2s.

Adoptive transfer of dead tumor cell-loaded cDC1s is more effective than cDC2s for therapeutic cancer treatment

We compared the efficacy of the optimized cDC1 and cDC2 anti-cancer vaccines to control the progression of established tumors. First, B16-OVA melanoma cells were intravenously injected into mice before administration of B16-OVA-loaded cDC anti-cancer vaccines (Fig. 2a–c). A single cDC1 treatment efficiently curtailed experimental tumor growth in the lung as compared with control mice. However, the cDC2 anti-cancer vaccine only mildly reduced tumor burden (Fig. 2b, c). Of note, the migration of cDC2s does not seem to be suboptimal as we recovered slightly higher numbers of cDC2s than cDC1s in popliteal LNs after their administration into the footpad of mice (Supplementary Fig. 2f, g). Next, cDC1 and cDC2 vaccines were prepared using MC38 TCL to treat mice previously grafted subcutaneously with MC38 cancers (Fig. 2d). cDC1 prime and boost administration reduced MC38 tumor growth versus controls, resulting in complete cancer rejection in 50% of animals. Treatment with the cDC2 anti-cancer vaccine initially halted MC38 cancer growth, but tumors finally outgrew. This led to a significantly lower survival rate in cDC2- compared with cDC1-treated mice (Fig. 2e, f).

Our results reveal that splenic cDC1-based anti-cancer vaccines are highly effective and superior to cDC2s in limiting established cancer progression.

Treatment with dead tumor cell-loaded cDC1s results in enhanced cancer prophylaxis compared to cDC2s

After having established the potency of cDC-induced anti-cancer effector T cell immunity for cancer therapy, we assessed the generation of cancer-controlling immune memory by cDC1- and cDC2-based anti-cancer vaccination. Naive mice were treated with cDC1s or cDC2s 30 days before B16-OVA or MC38 tumor cell injection and cancer progression monitored. We administered decreasing numbers of cDCs for a quantitative characterization of dose-dependency. Notably, cDC1s potently prevented B16-OVA outgrowth in the lung at every tested dose as compared with the control, indicating their maximal efficacy is already reached with very low cell numbers. cDC2s only effectively limited tumor growth at the highest tested dose (Fig. 3a, b). Similarly, cDC1-based vaccines controlled subcutaneous MC38 cancer outgrowth more effectively than cDC2 vaccines. Administration of high cDC2s numbers mildly extended survival of mice as compared with controls, but treatment with lower cDC2 numbers had no effect. However, every tested dose of the cDC1 anti-cancer vaccine reduced MC38 tumor growth and extended survival of mice (Fig. 3c–e).

Next, to investigate the role of endogenous cDC1s for the anti-cancer efficacy of cDC1 vaccination, we used XCR1^{DTRvenus} mice, which allow the temporal depletion of host cDC1s by injection of Diphtheria toxin (DT, Fig. 3f, g)[49]. Notably, treatment of XCR1^{DTRvenus} recipient mice with DT before and during the time of prophylactic cDC1 vaccination did not significantly alter the protective effect of adoptively transferred cDC1s against B16-OVA tumors (Fig. 3h). This observation suggests a limited contribution of endogenous cDC1s to the potential of cDC1 vaccines to induce cancer-controlling immune memory, which is in line with earlier findings assessing the priming of effector T cell responses[24].

In summary, we show that prophylactic dead tumor cell-loaded cDC anti-cancer vaccinations can halt tumor outgrowth after subsequent tumor challenge, with cDC1s being notably more efficient than cDC2s on a per cell basis and acting independently of host cDC1s.

cDC1-based anti-cancer vaccination has a higher potential for memory T cell generation than cDC2 vaccines

The superior efficiency of cDC1s compared to cDC2s in prophylactic cancer treatment suggests their enhanced capacity for long-lasting

https://doi.org/10.1038/s41467-025-58289-1

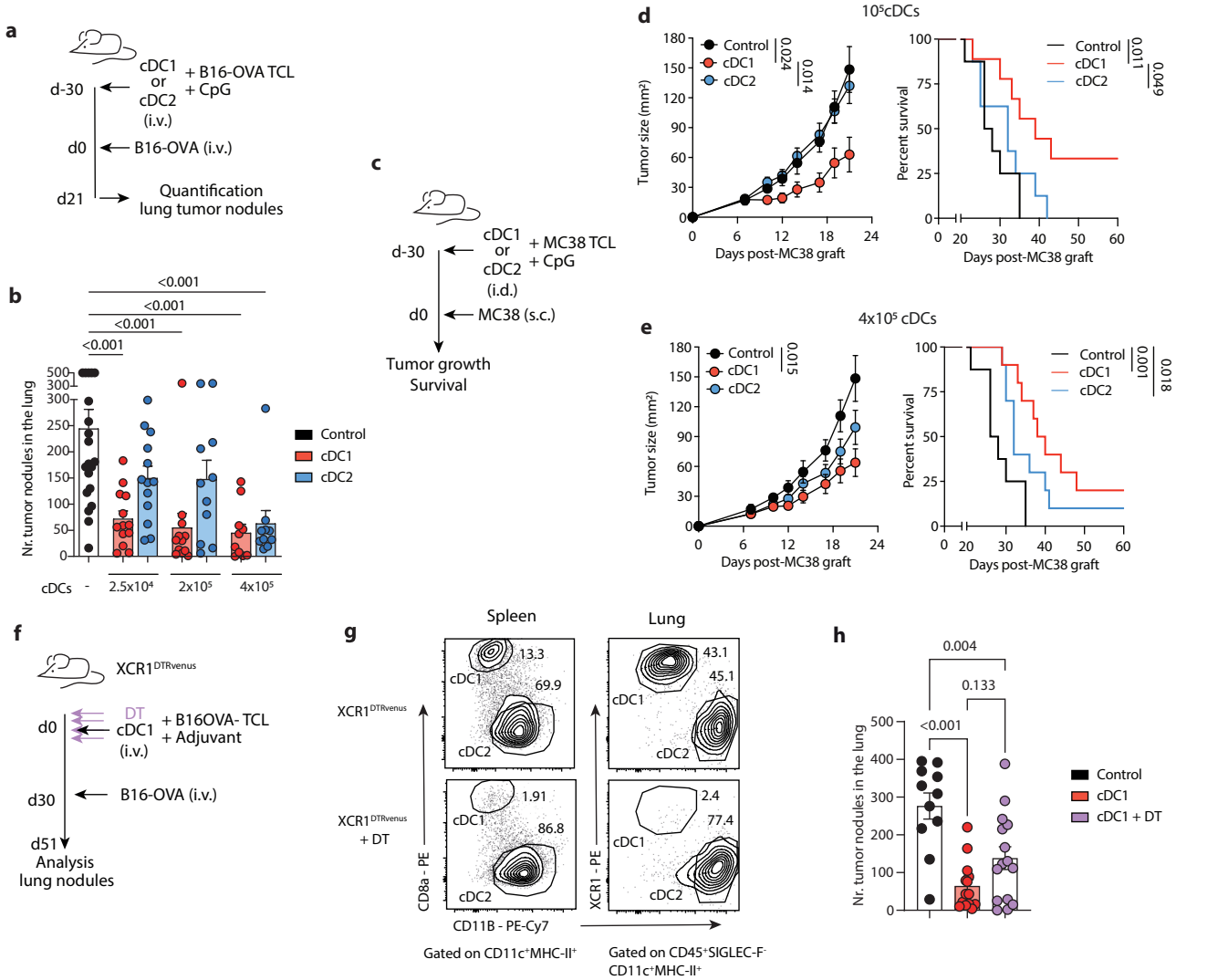

Fig. 3 | Treatment with cDC1s results in more effective prophylactic anti-cancer vaccination than cDC2 administration. a Experimental overview for (**b**): Control PBS or 2.5×10^4, 2×10^5 or 4×10^5 B16-OVA-TCL+CpG-pulsed splenic cDC1s or cDC2s were intravenously (i.v.) injected into naive mice. 30 days later, 4×10^5 B16-OVA cells were i.v. injected and lungs harvested 21 days thereafter. **b** Counts of tumor nodules on the lung surface are shown (left to right: $n = 20, 13, 12, 10, 13, 11, 10$ biological replicates/group from 3 independent experiments). **c** Experimental overview for (**d**, **e**), Control PBS or MC38-TCL+CpG-pulsed splenic cDC1s or cDC2s were intradermally (i.d.) injected into naive mice. 30 days later, 5×10^5 MC38 cells were subcutaneously (s.c.) injected into the right flank. **d**, **e** Tumor growth and humane endpoint determined after prophylactic i.d. injection of 10^5 (**d**) or 4×10^5 (**e**) cDCs are shown ($n = 8$ [control], 9 [10^5 cDC1], 10 [4×10^5 cDC1], 8 [10^5 cDC2], 10 [4×10^5 cDC2] biological replicates/group from 2 independent experiments). **f** Experimental overview for (**g**, **h**): XCR1^{DTRvenus} mice were treated with diphtheria toxin (DT) at days −2, −1, 0, 2 and vaccinated i.v. with 2×10^5 B16-OVA-TCL loaded cDC1s at day 0 or injected with control PBS. 30 days later, 4×10^5 B16-OVA cells were i.v. injected and lungs harvested 21 days thereafter. **g** Representative flow cytometry plots of cDC1 and cDC2 presence in the spleen (left) and lung (right) of XCR1^{DTRvenus} mice inoculated or not with DT at day 0 (just before cDC1 vaccination). **h** Counts of tumor nodules on the lung surface are shown ($n = 11$ [control], 14 [cDC1], 15 [cDC2] biological replicates/group from 2 independent experiments). Data are presented as mean ± SEM (dots represent individual data points). Statistical analysis by one-way ANOVA and Tukey post hoc test (**b**, **h**), two-way ANOVA (**d**) and Mantel-Cox test (**e**). Source data are provided as Source Data file.

anti-cancer immune memory priming. Hence, we analyzed the generation of tumor antigen-specific memory CD8$^+$ T cells by cDC vaccines. CD45.1$^+$ CD8$^+$ OT-I T cells were inoculated into mice prior to intravenous injection of different doses of B16-OVA TCL-loaded cDC1s or cDC2s and assessed after the T cell effector response had ceased (Day 30, Fig. 4a). OT-I T cells in the mediastinal lymph node (mdLN) and spleen largely differed phenotypically between control and cDC-treated mice, despite similar total numbers (Supplementary Fig. 3). Indeed, antigen experienced CD44$^+$ OT-I T cells were more abundant in all analyzed organs of mice treated with high numbers of cDC1s compared with mice vaccinated with cDC2s or control mice. Particularly in the mdLN, the low dose cDC1 anti-cancer vaccine also increased the presence of antigen experienced CD44$^+$ OT-I T cells (Fig. 4b, c).

Next, we injected B16-OVA TCL-loaded cDCs intradermally into previously OT-I cell-administered mice and analyzed the formed tumor antigen-specific CD8$^+$ memory T cells in the auricular LN (auLN) 25 days after the last treatment (Fig. 4d). cDC1-vaccinated mice harbored a greater frequency of OT-I T cells compared to cDC2-vaccinated and untreated mice (Fig. 4e). Moreover, the abundance of endogenous antigen-experienced CD44$^+$ CD8$^+$ and CD4$^+$ T cells in the auLN that produced IFNγ upon restimulation with OVA was also significantly elevated in the cDC1-vaccinated group (Fig. 4f, g).

These observations demonstrate that cDC1s are more effective than cDC2-based anti-cancer vaccination in the generation of tumor antigen-specific CD4$^+$ and CD8$^+$ memory T cells, a key feature of successful immunotherapies to prevent tumor recurrence.

https://doi.org/10.1038/s41467-025-58289-1

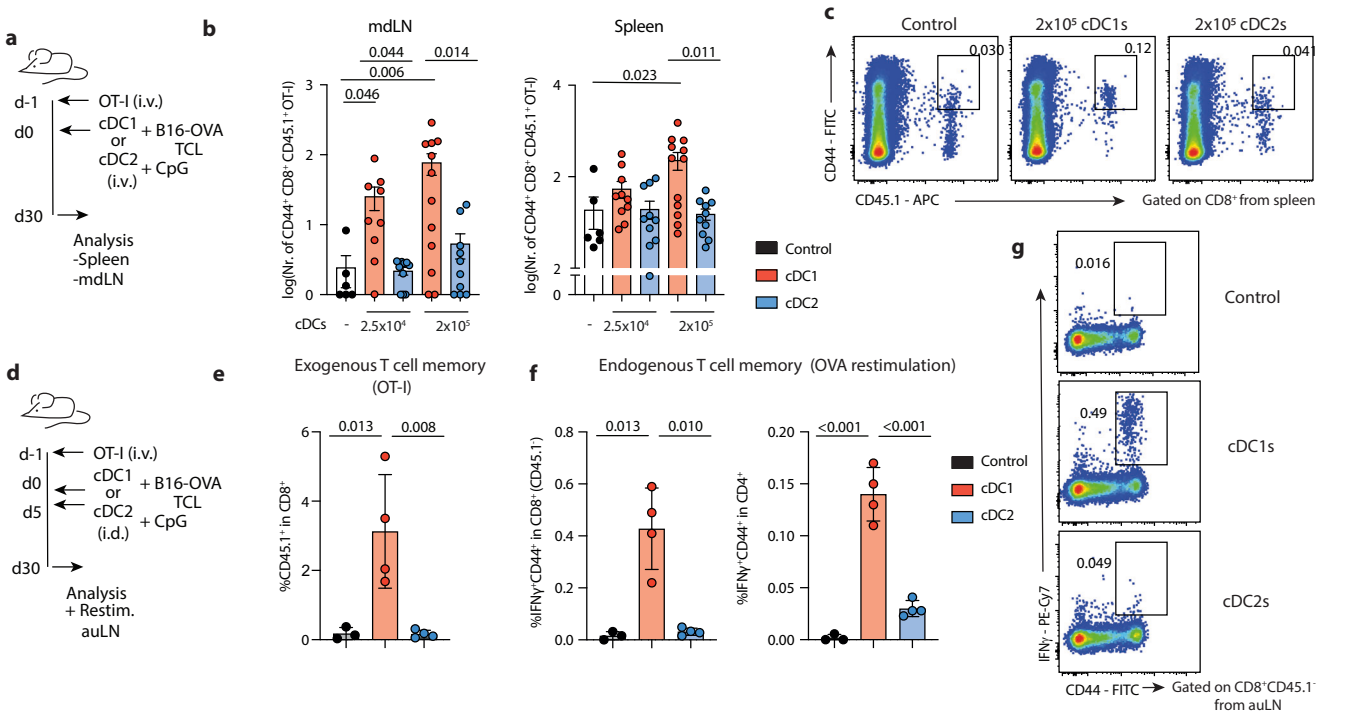

Fig. 4 | Dead tumor cell-loaded cDC1s are superior in induction of anti-cancer T cell memory compared with cDC2s. a Experimental overview for (**b**, **c**): naive mice were i.v. injected with 3×10^5 naive CD45.1$^+$ CD44$^-$ CD62L$^+$ CD8$^+$ OT-I T cells and, the following day, 2.5×10^4 or 2×10^5 B16-OVA TCL+CpG-pulsed splenic cDC1s or cDC2s or control PBS were i.v. administered. 30 days thereafter, spleen and mediastinal lymph node (mdLN) were analyzed by flow cytometry. **b** Numbers of antigen experienced CD44$^+$ CD45.1$^+$ CD8$^+$ OT-I T cells in tissues of mice are shown (left to right: $n = 6, 9, 10, 11, 10$ [mdLN]; 6, 10, 10, 11, 10 [spleen] biological replicates/group from 2 independent experiments). **c** Representative flow cytometry plot of the spleen of control mice or mice treated with 2×10^5 cDC1s or cDC2s (gated on alive CD3$^+$ CD8$^+$). **d** Experimental overview for (**e**–**g**): naive mice were i.v. injected with naive CD45.1$^+$ CD44$^-$ CD62L$^+$ CD8$^+$ OT-I T cells one day prior to intradermal prime and boost administration (in the ear) of control PBS, 10^6 cDC1s or cDC2s pulsed with CpG+B16-OVA TCL 5 days apart. The draining auricular lymph node (auLN) was restimulated with OVA protein and analyzed after 30 days by flow cytometry ($n = 3$ [control], 4 [cDC1], 4 [cDC2] biological replicates/group from one experiment). **e** Frequency of CD45.1$^+$ OT-I cells in CD8$^+$ T cells in the auLN is shown. **f** Frequency of endogenous IFNγ$^+$ CD44$^+$ within total CD45.1$^-$ CD8$^+$ (left) or CD4$^+$ (right) T cells in the auLN upon restimulation with OVA protein is shown. **g** Representative flow cytometry plot of OVA-restimulated endogenous CD45.1$^-$ CD8$^+$ T cells in the auLN. Data are presented as mean ± SEM (dots represent individual data points). Statistical analysis by one-way ANOVA and Tukey post hoc test. Source data are provided as Source Data file.

Adjuvant and neoadjuvant treatment with dead tumor cell-loaded cDC1s protects against experimental tumor relapse

To test the potential of cDC1-based vaccination to prevent tumor recurrence through T cell memory induction, we designed an experimental cancer relapse model in mice. Mice were grafted with MC38 tumors followed by tumor resection. Before (neoadjuvant) or after (adjuvant) surgery, mice received MC38 TCL-loaded cDC1s or the standard-of-care anti-PD1 blocking antibody[50] in a prime and boost scheme or were kept as untreated controls. 30 days after the last treatment, mice were re-challenged with MC38 cells, and secondary tumor growth and survival were monitored (Fig. 5a, b). The progression of the experimental relapse tumor indicates the capacity of the tumor-specific immune memory generated by a resected primary tumor and administered immunotherapies. Tumor-naive mice served as a further control to account for the effect of natural anti-cancer immune memory that is formed in tumor-resected mice which were otherwise untreated.

Firstly, we observed a significant delay in secondary MC38 tumor growth and an extended survival in untreated tumor-resected mice compared with naive mice. Secondly, mice treated with anti-PD1 in either the adjuvant or neoadjuvant setting displayed similar progression of a secondary re-challenge MC38 tumor as control untreated tumor-resected mice (Fig. 5c–f). Of note, the used anti-PD1 treatment scheme was effective and had a therapeutic effect on primary MC38 tumor progression in non-resected mice (Supplementary Fig. 4a, b). Thirdly, neoadjuvant and adjuvant cDC1 vaccination significantly protected mice from experimental cancer relapse. Indeed, up to 100% of mice treated with cDC1s fully rejected the re-challenge MC38 tumor (Fig. 5c–f), indicating higher anti-cancer immune memory generation by cDC1 immunotherapy than any other intervention. No protection against an unrelated tumor (B16-OVA) was observed in the untreated or cDC1-treated secondary MC38 tumor survivors compared to naive mice (Supplementary Fig. 4c, d), which further suggests a cancer antigen-specific immune memory response. In addition, we confirmed the efficacy of neoadjuvant cDC1 vaccination to prevent experimental cancer relapse after primary tumor resection using the aggressive B16-F10 melanoma model that does not respond to anti-PD1 blockade therapy[14]. In a comparable experimental setting (Fig. 5g), cDC1 treatment before surgery significantly reduced the growth of secondary relapse B16-F10 tumors compared with untreated cancer-experienced controls (Fig. 5h, i). This suggests a remarkable capacity of cDC1 vaccines to generate a protective anti-tumor immune memory even in poorly immunogenic cancers.

Next, we used blocking antibodies to assess the requirement of CD4$^+$ and CD8$^+$ T cells for the neoadjuvant cDC1-vaccination-induced rejection of secondary MC38 tumors. As previously, mice were grafted with MC38 tumors and treated with cDC1s in the neoadjuvant setting followed by tumor resection. CD4$^+$ or CD8$^+$ cells were temporally depleted shortly before injection of experimental relapse tumors into mice and cancer progression monitored (Fig. 5j and Supplementary Fig. 4e, f). We observed that depletion of CD4$^+$ cells did not affect the neoadjuvant cDC1-vaccination-mediated rejection of secondary MC38

https://doi.org/10.1038/s41467-025-58289-1

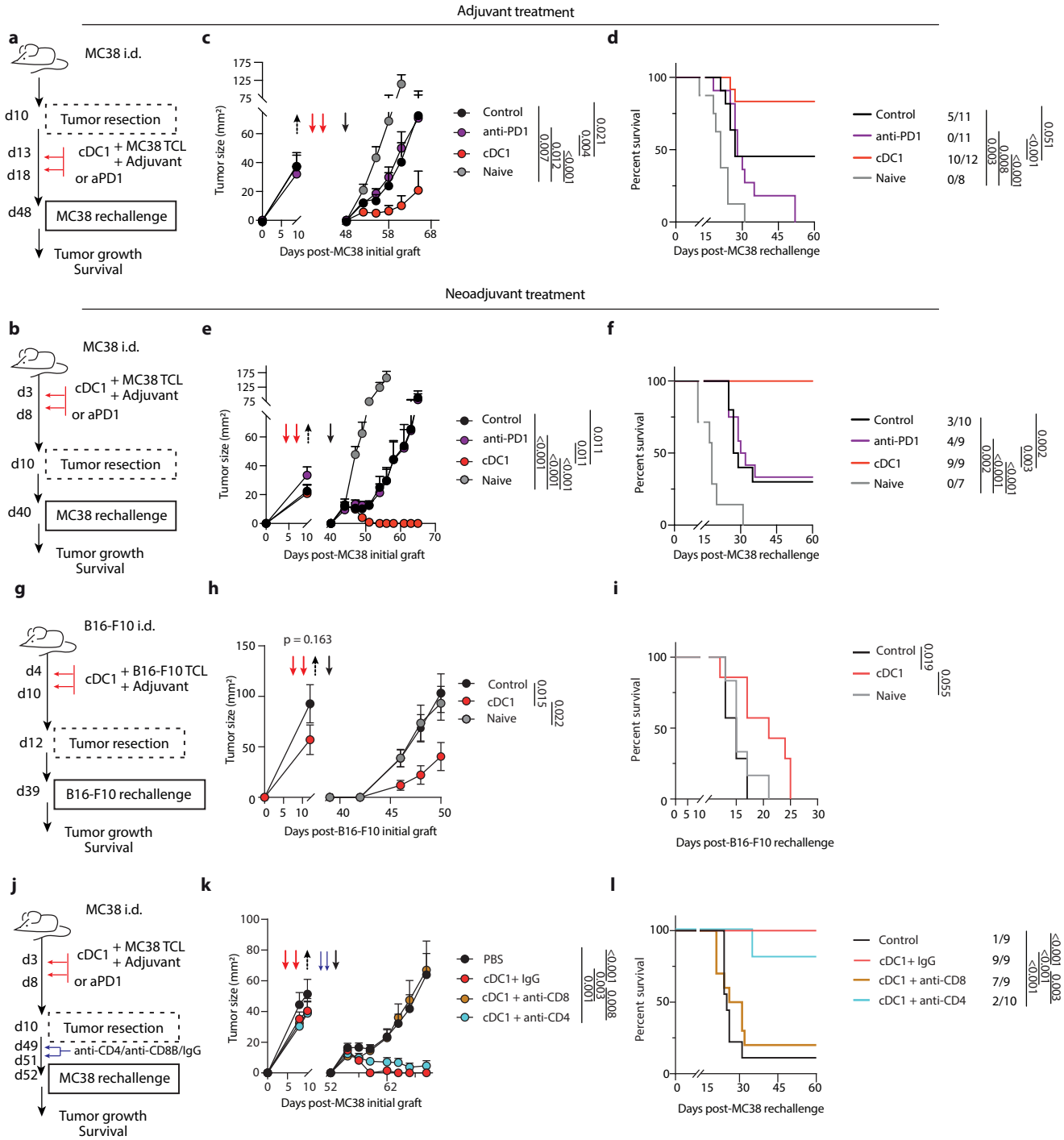

Fig. 5 | cDC1 anti-cancer vaccination blocks experimental cancer recurrence after tumor resection. a, **b** Experimental overview for (**c**–**f**): $5{\times}10^5$ MC38 cells were intradermally (i.d.) injected into naive mice (flank), and cancer growth monitored until day 10, when tumors were resected. Mice received adjuvant (post-surgery, day 13 and 18) (**a**, **c**, **d**) or neoadjuvant (pre-surgery, day 3 and 8) (**b**, **e**, **f**) treatments with anti-PD1 antibody intraperitoneally (i.p.), 10^6 MC38-TCL loaded cDC1s (i.d.), or PBS control. 30 days after the last intervention, 1.5×10^6 MC38 cells were reinjected (same flank) and tumor growth (**c**, **e**) and survival (**d**, **f**) monitored. Tumor naive mice only received MC38 cells at day 48 (**c**, **d**; $n = 11$ [control], 11, [anti-PD1], 12 [cDC1], 8 [naïve]) or 40 (**e**, **f**; $n = 10$ [control], 12, [anti-PD1], 9 [cDC1], 7 [naïve]). n represents biological replicates/group from 2 independent experiments). **g** Experimental overview for (**h**, **i**): 10^5 B16-F10 cells were i.d. injected and on day 12 tumors were resected. On days 4 and 10, mice were treated with B16-F10-TCL loaded cDC1s (10^6, i.d.), or control PBS. On day 39, 7×10^5 B16-F10 cells were i.d. injected in the same flank, and tumor growth (**h**) and survival (**i**) monitored. Tumor naive mice were only injected with 7×10^5 B16-F10 cell at day 39 ($n = 6$ [control], 7 [cDC1], 7 [cDC2] biological replicates/group from one experiment). **j** Experimental overview for (**k**, **l**): 5×10^5 MC38 cells were i.d. injected and on day 10 tumors were resected. On days 3 and 8, mice were treated with MC38-TCL loaded cDC1s (10^6, i.d.), or control PBS. At day 49 and 51 after the initial tumor graft, cDC1-treated mice were injected with anti-CD4, anti-CD8b depleting antibodies or rat IgG as control i.p. On day 52, 1.5×10^6 MC38 cells were i.d. injected in the same flank of mice, and tumor growth (**k**) and survival (**l**) monitored ($n = 9$ [control], 9 [cDC1+IgG], 10 [cDC1+anti-CD8], 9 [cDC1+anti-CD4] biological replicates/group from 2 independent experiments). Data are presented as mean ± SEM. Statistical analysis by two-way ANOVA (c, e, h, k) and Mantel-Cox test (**d**, **f**, **i**, **l**). Source data are provided as Source Data file.

tumors. Unfortunately, additional to CD4+ anti-cancer effector T cells, those mice also lack CD4+ Tregs (Supplementary Fig. 4e, f) with their potent pro-cancer functions[51]. The cancer control by CD4+ cell-depleted mice is likely caused by a loss of Tregs, which complicates drawing conclusions about the potential role of other CD4+ T cell subsets that may, conversely, contribute to tumor rejection. Notably, the neoadjuvant cDC1 vaccination-induced protection against experimental relapse MC38 tumors was completely blunted upon loss of CD8+ T cells (Fig. 5k, l). This finding highlights CD8+ T cell immunity as ultimate effector of cDC1-induced cancer-protective immune memory.

Overall, these data show that adjuvant and neoadjuvant cDC1 immunotherapy notably reduces tumor recurrence compared with anti-PD1 treatment and indicate an improved induction of anti-tumor immune memory in tumor-bearing or -resected hosts by cDC1s.

Neoadjuvant cDC1 vaccination boosts a unique CD4+ memory T cell signature that precedes rejection of relapsing tumors

We examined the immune response leading to secondary tumor rejection in neoadjuvant cDC1 immunotherapy-treated mice to characterize the generated T cell memory. To this end, the myeloid and lymphoid infiltrate of MC38 tumors in the experimental relapse mouse model (Fig. 5b) was analyzed at day 5 post re-challenge (Fig. 6a). No significant alteration in the myeloid compartment in the TME of secondary tumors was found except of lower monocyte and higher macrophage numbers in cancer-resected mice compared with naïve mice (Supplementary Fig. 5a, b). In contrast, higher frequencies of CD4+ and CD8+ tumor infiltrating lymphocytes (TILs) were found in neoadjuvant cDC1-treated mice compared with other therapy or control groups (Fig. 6b and Supplementary Fig. 5c). Next, we sorted CD4+ and CD8+ TILs from secondary MC38 tumors and performed a 3' mRNA single-cell transcriptome analysis (scRNAseq). TILs clustered in 13 subsets (Fig. 6c) that were annotated on the basis of classical T cell marker expression[52], the most deregulated genes per cluster (Supplementary Fig. 6a-c), cross-labeling with prior annotation of scRNA-seq data from MC38-derived TILs[53] and human TILs[54]. This analysis identified four major populations of CD8+ TILs: effector memory (Tem), central memory (Tcm), Tcm with high expression of KLR genes (Tcm KLR), and tissue resident memory cytotoxic (Trm cytotoxic); and four major CD4+ TIL clusters: Tem, CD4+ T cells expressing IL7R (Teff IL7R), regulatory (Treg) and tissue resident memory-like (Trm). The most abundant cluster were CD4+ Trm-like cells (CD4+ Trm) that we annotated based on their unique expression of hallmark genes for tissue resident memory T cells (high *Cd44*, *Cd69*, *Cxcr6*, *Bhlhe40*, and *Icos*; and low *Sell*, *Ccr7*, *S1pr1*, *Tcf7*, and *Klf2*[55]) (Fig. 6d and Supplementary 6a-c).

We then evaluated the composition of the T cell compartment in our experimental conditions. Secondary tumors of mice from which a primary tumor was resected contained more TILs compared to tumors from naive mice, which indicates that pre-exposure to a tumor generates natural anti-tumor immunity characterized by the presence of Trm cells (Fig. 6e, f). The presence of CD4+ and CD8+ TIL subsets in secondary tumors of control and neoadjuvant anti-PD1-treated mice was similar, apart from higher frequencies of CD8+ cytotoxic Trms upon anti-PD1 treatment (Fig. 6e, f). This T cell subset has been associated with improved prognosis of cancer patients[54], however, we did not observe such a correlation with enhanced cancer remission in secondary MC38 tumors (Fig. 5e, f). Notably, all other CD8+ TIL subsets were specifically enriched in secondary tumors of mice treated with neoadjuvant cDC1 vaccination, particularly the CD8+ Tcm and Tem subpopulations (Fig. 6e, f). An increased presence of CD8+ TILs is generally associated with a better prognosis in human patients with cancer[56]. Hence, the observed elevated intratumoral CD8+ T cell infiltration likely explains why the complete rejection of secondary re-challenge tumors in neoadjuvant cDC1-treated mice depends on CD8+ cells (Fig. 5j–l).

Additionally, the presence of CD4+ TILs was also higher in secondary tumors of cDC1-vaccinated versus other groups. The 15-fold induction of CD4+ Trm cell frequencies in re-challenge tumors was the most clear-cut difference upon neoadjuvant cDC1 treatment compared to control or anti-PD1 therapy. CD4+ Tem presence was also elevated in cDC1-treated secondary tumors, while the abundance of other T cell clusters was not notably changed between treatment groups (Fig. 6e, f).

To further assess the intrinsic potential of cDC1 vaccines to generate CD4+ Trms, we injected $XCR1^{DTRvenus}$ mice with DT to deplete host cDC1s (Supplementary Fig. 6d) and, subsequently, treated the mice intradermally with B16-OVA TCL-loaded cDC1s (Fig. 6g). 30 days thereafter, we observed that cDC1 vaccination induced both, CD69+ CXCR6+ or CD103- CD8+ Trms and CD69+ CXCR6+ or CD103- CD4+ Trms, in the skin, which was independent of the presence of endogenous cDC1s during vaccination (Fig. 6g–i and Supplementary 6d,e).

To gain insights into the potential activities of CD4+ Trms in the TME of experimental relapse tumors, we analyzed functional gene expression of CD4+ T cell subset clusters (Fig. 6c). Compared to other CD4+ T cell clusters, CD4+ Trm cells displayed a significantly higher metabolic activity (Fig. 6j) and increased expression of key genes fostering their proximity to cDCs (e.g., *Cxcr6*, Fig. 6d), migration (e.g., *Ccr2*, *Ccr5*), cDC activation and survival (e.g., *CD40lg*), and licensing of CD8+ T cell activation (e.g., *Ifng*, *Tnf*, *Pdcd1*, *Lag3*, *Havcr2*, *Tnfrsf4*, *Tnfrsf9*) (Fig. 6k). This is in line with the particular potency of cDC1s to foster IFNγ+ CD44+ CD4+ effector and memory T cell responses (Figs. 1h and 4f). Hence, the abundance of CD4+ Trms expressing cDC1-interaction and CD8+ T cell-activating genes in concert with higher numbers of CD8+ T cells in secondary tumors of cDC1-treated mice suggests that vaccine-induced CD4+ T cells promote the persistence of CD8+ T cells.

In summary, these data indicate that the protective immunity conferred by neoadjuvant cDC1 vaccination in the context of tumor recurrence results not only in the augmented presence of memory CD8+ TILs but also in a unique CD4+ T cell signature in secondary tumors that precedes their remission. Those cDC1-induced CD4+ TILs are characterized by a great boost in effector, memory and, particularly, a tissue resident memory phenotype.

The abundance of CD4+ Trm cells in human tumors correlates with intratumoral cDC1 presence and enhanced patient survival

CD4+ T cells with a Trm phenotype were reported previously in human tumors by scRNAseq analysis[54,57]. To determine a potential link between cDC1s and CD4+ Trm in patients with cancer, we analyzed whether cDC1 abundance associates with CD4+ Trm presence in human tumors using three different approaches. First, we defined a gene signature for CD4+ Trms that comprises the significantly upregulated genes in CD4+ Trms compared to other T cell clusters in secondary tumors in mice (Supplementary Fig. 6b and Supplementary Table 1), which we refer to as cDC1-induced CD4+ Trm signature. Additionally, we used a signature of upregulated genes in the CD4+ CD103+ TIL cluster in human breast carcinoma (BRCA) that the authors also denote as CD4+ Trm[54], which we refer to as human BRCA CD4+ Trm signature (Supplementary Table 1). Notably, we found a significant correlation between both CD4+ Trm gene signatures and an established cDC1 gene signature[32] in transcriptomic data of human skin melanoma (SKCM) and BRCA from the Cancer Genome Atlas (TCGA)[58] (Fig. 7a, b).

Second, we investigated the actual frequencies of cDC1s and CD4+ Trms in human tumors. We used publicly available scRNAseq data from 22 BRCAs (GSE176078[59]) that include data on myeloid and lymphoid cells. The authors already annotated an intratumoral cDC1:CLEC9A cluster that represents cDC1s. CD4+ Trms were not detected in BRCA in the initial analysis by the authors[59] (Supplementary Fig. 7a), likely due to the low abundance of CD4 Trms in tumors. For an in-depth

https://doi.org/10.1038/s41467-025-58289-1

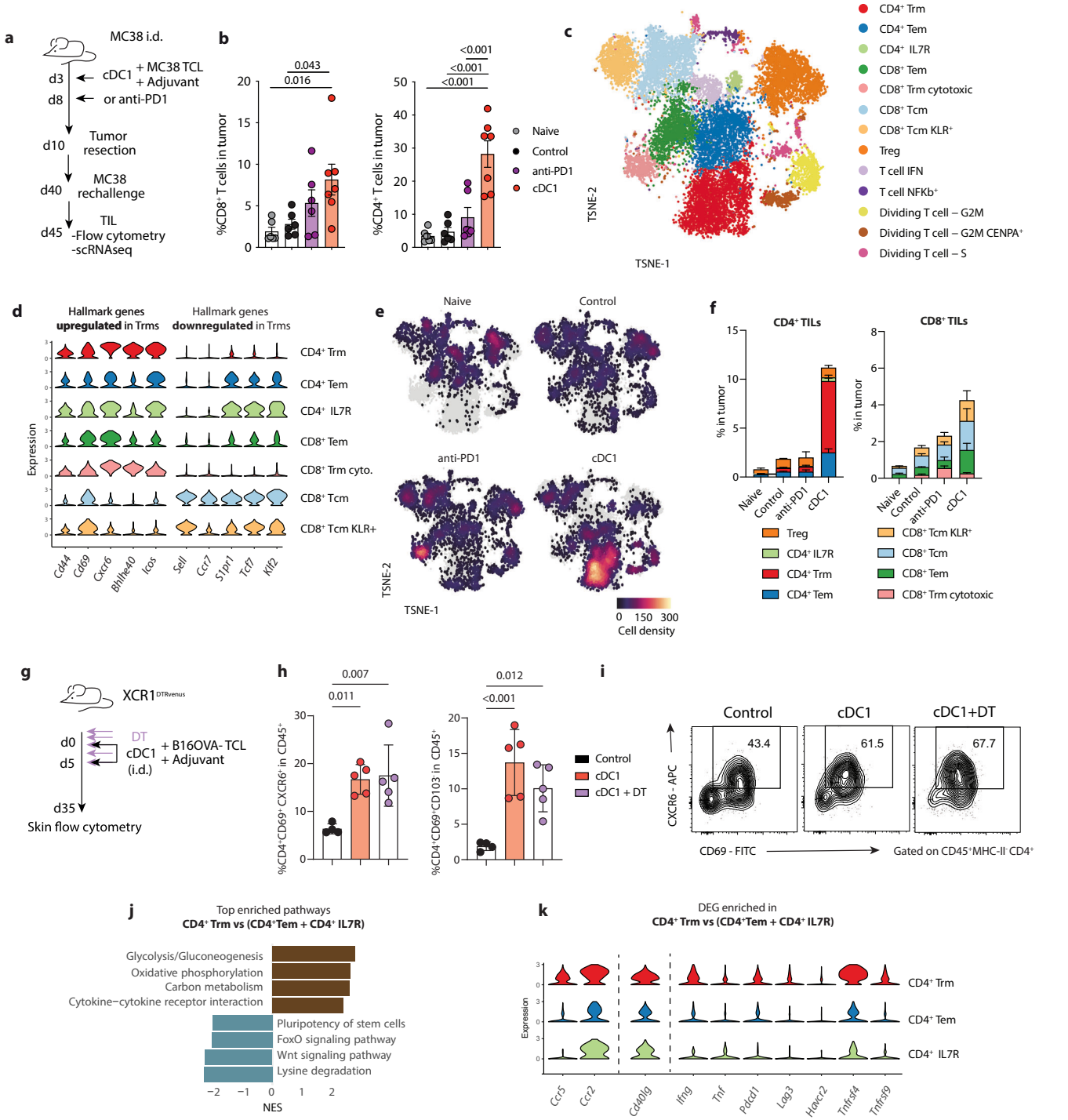

Fig. 6 | Neoadjuvant cDC1-based vaccination enhances CD8⁺ and CD4⁺ memory T cell responses upon tumor recurrence. a Experimental overview for (**a**–**h**): Mice grafted with MC38 cells (i.d.) were injected at day 3 and 8 with control PBS, anti-PD1 antibody or 10^6 MC38-TCL loaded cDC1s (i.d), and tumors resected at day 10. 30 days later, mice were re-challenged with MC38 cells. Tumor naive mice only received MC38 cells at day 40. Secondary tumors were analyzed on day 5 after grafting. **b** Frequency of CD8⁺ or CD4⁺ T cells in secondary MC38 tumors ($n = 6$ or 7 [cDC1] biological replicates/group of one representative of two independent experiments). **c** CD45⁺ and CD8⁺ or CD4⁺ T cells sorted from secondary MC38 tumors and analyzed by scRNAseq (2 replicates per condition). Multiparametric t-SNE representation and annotation is shown. **d** Violin plots of tissue resident memory (Trm) hallmark gene expression within most abundant T cell clusters from (**c**). **e** t-SNE plot with distribution of T cells for each experimental group. Grey dots show all detected cells, black to yellow-colored areas show T cell density/ experimental group. **f** Frequency of the most abundant clusters within secondary MC38 tumors ($n = 2$ biological replicates pooling 3 mice/group). **g** Experimental overview for (**h**, **i**): XCR1^{DTRvenus} mice received diphtheria toxin (DT) at days −2, −1, 0, 2, 5 i.p. and 10^6 B16-OVA-TCL loaded cDC1s or PBS at days 0 and 5 (i.d. in ear) before analysis of ear skin at day 30. Frequency of CD4⁺ CD69⁺ CXCR6⁺ and CD4⁺ CD69⁺ CD103⁻ Trms (**h**, $n = 4$ [control], 5 [cDC1], 5 [cDC1+DT] biological replicates/group, representative experiment from 2 independent experiments) and representative flow cytometry plots (**i**, gated on CD45⁺ CD4⁺ cells) are shown. **j** Ranked pathway enrichment analysis comparing gene expression of CD4⁺ Trms with cells of CD4⁺ Tem and CD4⁺ IL7R clusters. **k** Violin plots showing expression of genes significantly (adj p value ≤0.001) enriched in CD4⁺ Trms of analysis in (**j**). Data are presented as mean ± SEM (dots represent individual data points) unless indicated otherwise. Statistical analysis by one-way ANOVA and Tukey post-hoc test (**b**, **h**) and Wilcox test (**k**). Source data are provided as Source Data file.

https://doi.org/10.1038/s41467-025-58289-1

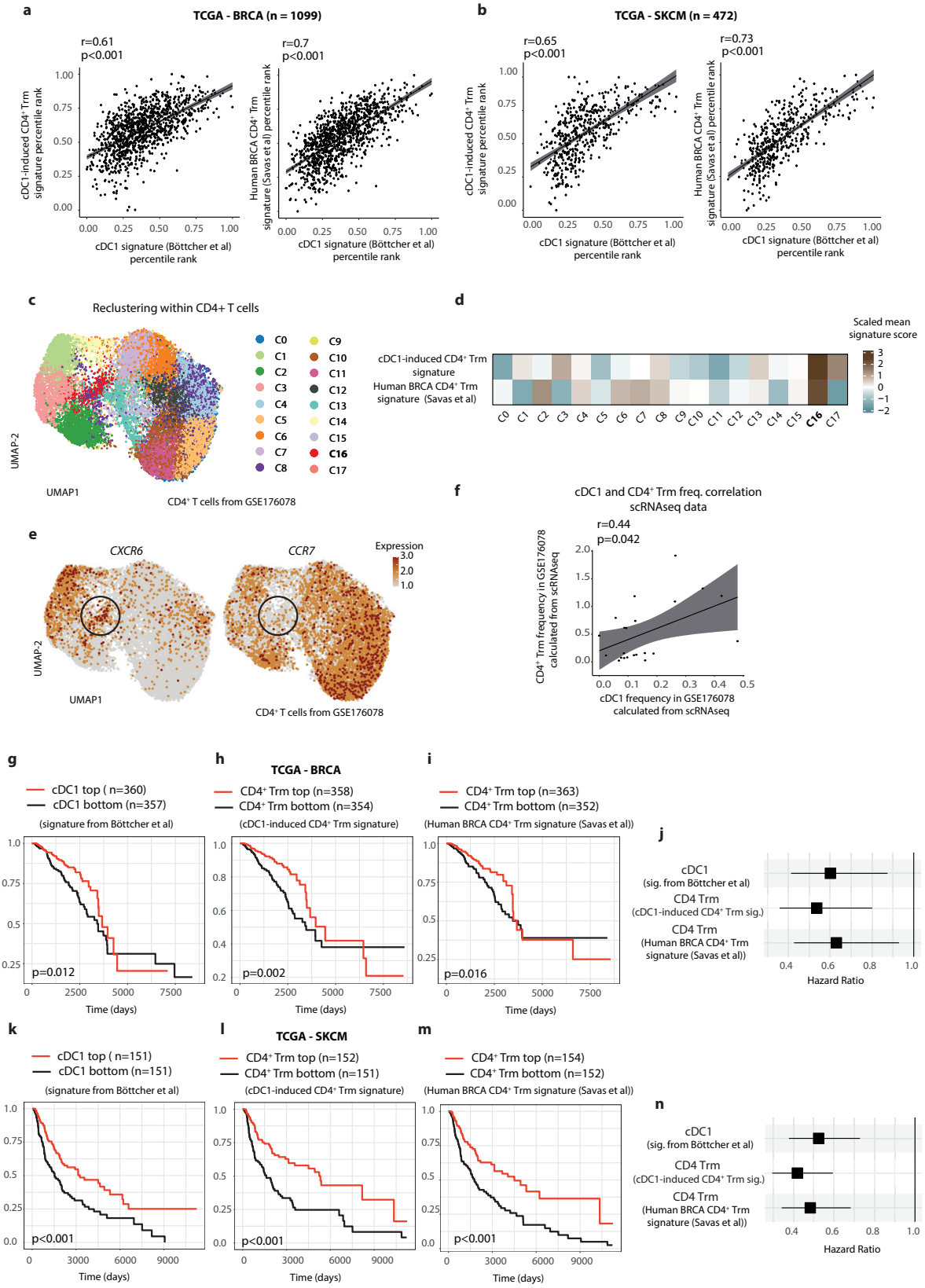

examination, we re-clustered the 22,247 CD4$^+$ TILs and identified 17 CD4$^+$ T cell sub-clusters (Fig. 7c). To identify CD4$^+$ Trms, we analyzed the expression of the cDC1-induced CD4$^+$ Trm and human BRCA CD4$^+$ Trm signatures (Supplementary Table 1) within each sub-cluster (Fig. 7d). Cells in sub-cluster 16 (C16) displayed the highest expression of both CD4$^+$ Trm gene signatures among all CD4$^+$ T cell sub-clusters. We confirmed the expression pattern of hallmark Trm genes in cells comprising C16; high expression of *CXCR6* and *PDCD1* and low expression of *CCR7*, *SELL*, and *TCF7* (Fig. 7e and Supplementary Fig. 7b). Therefore, we annotated the sub-cluster C16 of CD4$^+$ T cells in human BRCA as CD4$^+$ Trm. Finally, we analyzed the association of the frequency of CD4$^+$ Trm and cDC1:CLEC9A within all sequenced cells for

Fig. 7 | Intratumoral presence of CD4⁺ Trms correlates with cDC1 abundance and patient survival in BRCA and SKCM. a, **b** cDC1 scores based on the expression of *CLNK*, *BATF3*, *XCR1* and *CLEC9A* (cDC1 gene signature established in ref. 32) and CD4⁺ Trm scores based on the expression of the genes included in the cDC1-induced CD4⁺ Trm signature and the human BRCA CD4⁺ Trm signature[54] (Table S1) were calculated for breast carcinoma (BRCA) (**a**) or human skin melanoma (SKCM) (**b**) from the TCGA. The Pearson's correlations of cDC1 and CD4⁺ Trm scores normalized by percentile rank and the linear regression with a 95% confidence region are shown. **c** Uniform Manifold Approximation and Projection (UMAP) representing CD4⁺ T cells from 22 human BRCA patients (GSE176078[59],). The newly identified sub-clusters after re-clustering are shown. **d** Heatmap showing the scaled signature score of the cDC1-induced CD4⁺ Trm signature and the human BRCA CD4⁺ Trm signature[54] (Table S1) of cells contained in each of the 17 CD4⁺ T cell sub-clusters in human BRCA identified in (**c**). **e** UMAPs depicting the single cell expression of *CXCR6* (left panel) and *CCR7* (right panel) by cells contained within the CD4⁺ T cell clusters in human BRCA. Grey dots show the outline for the CD4⁺ T cell clusters and brown-colored dots indicate the level of expression for the respective gene by a cell. A black circle indicates the location of the CD4⁺ Trm sub-cluster C16. **f** The frequency of cells contained in the CD4⁺ Trm sub-cluster C16 (**c**–**e**) and the cDC1:CLEC9A cluster (identified in ref. 59) within all tumor cells was calculated for each BRCA patient ($n = 22$). The Pearson's correlation of intratumoral CD4⁺ Trm and cDC1 frequencies and the linear regression with a 95% confidence region are shown. **g**–**n** Survival curves of BRCA (**g**, **i**, **k**) and SKCM (**h**, **j**, **l**) patients from the TGCA with high or low (top and bottom tertiles, respectively) intratumoral cDC1 (**g**, **h**) or CD4⁺ Trm (**j**–**l**) scores calculated using gene signatures as in (**a**, **b**). Hazard ratio and 95% coefficient interval are indicated (**j**, **n**). Statistical analysis by Mantel-Cox test.

each human tumor. Notably, despite a low number of patients, we found a significant direct correlation between the presence of CD4⁺ Trms and cDC1s in human BRCAs (Fig. 7f).

Third, given the lack of markers exclusive to CD4⁺ Trms within its signatures, we confirmed our analysis in BRCA patients from the TCGA cohort[58] by deconvoluting cDC1 and CD4⁺ Trm frequencies using DigitalDLSorter[60] trained with whole-tumor scRNAseq data[59] (Supplementary Fig. 7c). Notably, those predicted cell frequencies of CD4⁺ Trms and cDC1s also showed a strong positive correlation in human BRCA (Supplementary Fig. 7d).

Next, we interrogated the predictive value of elevated intratumoral CD4⁺ Trm and cDC1 presence for the survival of cancer patients. As previously shown, we confirmed that high cDC1 signatures predicted improved overall survival (OS) of BRCA and SKCM patients (Fig. 7g–n)[32]. Notably, the increased presence of CD4⁺ Trms in the TME, when deconvoluted based on gene signatures or scRNAseq data, significantly correlated with BRCA and SKCM patient survival (Fig. 7g–n and Supplementary Fig. 7e). The hazard ratios of the higher number of cDC1s or CD4⁺ Trms in tumors are comparably low (Fig. 7j, n), which further suggested a functional connection between those two cell types.

Overall, we show that CD4⁺ Trm-like cells are present in human cancers, their elevated abundance correlates with that of cDC1s and serves as a significant predictor for patient survival. Our findings suggests that cDC1s are involved in the disease-relevant immunobiology of CD4⁺ Trms in human cancers.

Discussion

Comparative studies of mouse cDC1s and cDC2s isolated from tumors or generated from bone marrow in vitro for immunotherapy of primary tumors suggests their tumor context- and administration route-dependent efficacy[24,43]. Notably, those and other pre-clinical studies demonstrated that cDCs induce host-independent and superior anti-cancer effector immunity compared with monocyte-derived DCs (generated from the bone marrow with GM-CSF)[24,33], which are the basis for most current DC-based vaccination efforts in cancer patients[61]. However, in clinical practice, harvesting DCs from tumors appears cumbersome. Moreover, mouse in vitro Flt3L-differentiated cDC1- and cDC2-like cells have a reduced capacity for CD4⁺ T cell activation compared to splenic cDCs[62]. Notably, transcriptional and functional analyses confirmed that cDC1s and cDC2s from mouse spleen closely resemble their human counterparts[26,36].

We previously showed the efficacy of splenic cDC1 vaccination for controlling primary cancers[14]. Here, we optimized splenic cDC1 and cDC2 vaccination protocols using ICD-induced dead tumor cells as antigen source and compared their anti-tumor effects. Contrary to in vitro generated cDC2-like cells[24], treatment with TCL-loaded splenic cDC2s induced anti-tumor effector CD4⁺ and CD8⁺ T cell responses from the endogenous repertoire and decreased primary cancer progression in two pre-clinical models. This finding has relevant implications for the clinic as human circulating cDC2s are more abundant than cDC1s and reflects the capacity of human cDC2s to induce T cell immunity in cancer[17]. Nevertheless, we report the superior potential of TCL-loaded cDC1 vaccination to generate specific effector T cell immunity and control primary tumors compared to cDC2-based vaccination. While cDC1s cross present antigens to CD8⁺ T cells, our data also support their capacity for priming of tumor specific effector CD4⁺ T cells[27]. The differential immune priming between cDC1s and cDC2s can be partially due to higher capacity of cellular antigen uptake by cDC1s[63] and different, less universal, tumor antigens or agonists/adjuvants may improve the performance of cDC2s. The generation of long-lasting anti-tumor immune memory is critical to improve survival of patients with cancer. We demonstrated that the strong effector T cell response induced by cDC1 vaccination of tumor-bearing mice translates into the robust formation of a systemic CD8⁺ and resident CD4⁺ T cell immune memory, which prevents tumor recurrence. In fact, clinical trials are currently exploring the potential of plasmacytoid DC- and cDC2-based vaccines to limit tumor recurrence after primary tumor resection[16,17,40], although results from the first phase III next-generation vaccine trial showed no clinical benefits, despite measurable immune effector responses[42]. However, our pre-clinical data suggest the specific potency of cDC1-based vaccination, which outperformed cDC2s in protective CD4⁺ and CD8⁺ memory T cell induction.

PD1 blockade before and after tumor resection is a clinically effective cancer treatment, likely due to intact immune structures and abundant tumor antigen in tumors and reduced immunosuppression upon tumor surgery, respectively[64–66]. Hence, we compared cDC1-based vaccination with anti-PD1 therapy in clinically relevant neoadjuvant and adjuvant treatment regimens in mice. To this end, we developed a pre-clinical cancer resection model that recapitulates the formation of natural anti-cancer immunity due to primary tumor presence. This model allowed us to specifically assess the potency of the anti-cancer immune memory that is generated by immunotherapy beyond the natural immunity in tumor-resected hosts. Notably, in the neoadjuvant and adjuvant setting, adoptive transfer of dead tumor cell-loaded cDC1s significantly improved the control of secondary re-challenge tumors compared to anti-PD1 therapy and resulted in complete remission in almost all cDC1-treated mice. We additionally demonstrate the potency of neoadjuvant cDC1 vaccination to limit experimental cancer relapse in a second, poorly immunogenic mouse cancer model. Of note, the potential of cDC1 treatment to induce cancer-recurrence controlling memory responses is not inhibited in tumor-bearing hosts, which is a common concern for DC vaccines[67]. Overall, our results demonstrate the superior ability of cDC1-based vaccination to induce long-lasting anti-cancer immune responses and prevent tumor relapse than ICB immunotherapy.

The clinical potency of cancer-specific memory T cells for halting cancer recurrence is emerging, however therapeutic means for their induction are limited. Trms are long-lived T cells that reside permanently in tissues and provide protection against pathogens and cancer[55]. Transient PD1 blockade during acute infection promotes a

strong antigen-specific CD8⁺ effector and memory T cell response[68]. Consistently, we observed an enhanced cytotoxic CD8⁺ Trm cell presence in secondary re-challenge tumors of mice treated with neoadjuvant anti-PD1 compared to control or cDC1-treated mice. High intratumoral CD8⁺ Trm presence is associated with an improved response to immunotherapy[69,70] and survival of patients with cancer[54]. Hence, promotion of CD8⁺ Trm formation is proposed to prevent tumor recurrence[11–13]. However, compared with controls, we did not observe an enhanced rejection of secondary tumors in mice treated with neoadjuvant anti-PD1, which harbor the highest numbers of CD8⁺ Trms. These data support the earlier suggestion that successful (neo-) adjuvant anti-PD1 immunotherapy in patients relies on killing of dormant tumor cells[71] rather than promoting immune memory.

Notably, we observed that TCL-loaded cDC1 vaccination leads to a systemic mobilization of anti-tumor memory T cells in mice. cDC1 administration to primary tumor-bearing mice before surgery triggered the increased presence of anti-tumor circulating and resident memory T cells in secondary re-challenge tumors prior to their complete rejection. Secondary tumors of neoadjuvant cDC1-vaccinated mice harbored the highest frequencies of effector and circulating memory CD8⁺ T cells. The presence of CD8⁺ T cells correlates with improved prognosis for cancer patients[6,7] and tumor-specific CD8⁺ Tcm are reactivated by cDC1s to fully active cytotoxic CD8⁺ T cells that protect mice from cancer outgrowth[13]. Indeed, we found that the 100% rejection rate of secondary re-challenge tumors in neoadjuvant cDC1-treated mice depended on CD8⁺ T cells. Additionally, we found a pronounced induction of CD4⁺ T cells with a Trm phenotype specifically in secondary tumors of neoadjuvant cDC1-treated mice. In general, the relevance of intratumoral CD4⁺ helper T cells to aid the interaction and anti-tumor activities of cDC1s and CD8⁺ T cells is emerging[72–74]. CD4⁺ Trms are found in non-lymphoid organs upon infection, where they rapidly secrete cytokines and recruit lymphocytes to the mucosa after antigen recognition[75]. Despite being poorly investigated, CD4⁺ T cells with a Trm phenotype are also present in human tumors[54,76]. Here, we show that the presence of intratumoral cDC1s correlates with CD4⁺ Trm abundance in human SKCM and BRCA. In line, recent preclinical studies report the enrichment of a CD4⁺ TIL population expressing Trm markers upon treatment with CD40 agonist, which activates DCs[53]. Trm marker-expressing CD4⁺ T cells preferentially interact with cDCs in human non-small cell lung cancer[77] as well as with cDC1s in colorectal cancer (CRC)[53], and their abundance associates with improved responses to ICB of CRC patients[78]. Notably, we show that CD4⁺ Trms highly express genes that foster their interaction with cDC1s and promote the activities of CD8⁺ T cells. Accordingly, secondary tumors of neoadjuvant cDC1-treated mice show the highest infiltration of both, CD4⁺ Trms and anti-cancer CD8⁺ T cells. In line, we found that an elevated presence of intratumoral CD4⁺ T cells with a Trm phenotype significantly associates with the prolonged overall survival of BRCA and SKCM patients. Our data support a crosstalk between cDC1s and CD4⁺ Trm-like cells and its functional importance for anti-cancer immunity, generation of anti-cancer immune memory, and prevention of tumor relapse. Moreover, this setting reveals an immunotherapeutic strategy to increase CD4⁺ Trm-like cells in tumors, which will aid their further study.

Here, we revealed that cDC1 immunotherapy drives superior effector and memory CD4⁺ and CD8⁺ responses compared to cDC2-based vaccines. We also demonstrated the efficacy of adjuvant and neoadjuvant cDC1-based vaccination to almost completely reject experimental relapse tumors via the generation of anti-cancer CD8⁺ and CD4⁺ T cell memory. This study reinforces the notion that anti-cancer vaccination strategies should be tailored towards promoting both, CD4⁺ and CD8⁺, T cell responses[79]. However, deciphering the origin, migration pattern, and the precise functional role of CD4⁺ Trm-like cells in the context of cancer warrants further research, for which cDC1 vaccination will be an effective experimental tool. Notably, the first phase I/II clinical trials administering (ex vivo tumor lysate-loaded and activated) circulating cDC1s alone or together with cDC2s to patients with ovarian cancer (NCT05773859) or melanoma[34] demonstrates the translatability of cDC1 anti-cancer vaccination. Our results argue for the use of cDC1-based anti-cancer immunotherapy in clinical practice in combination with cancer surgery to specifically tackle the urgent need to prevent tumor recurrence in patients.

Methods

Study design

The objective of this study was to investigate the anti-tumor potential of natural cDC1 and cDC2-based vaccination and explore the anti-tumor specific immune memory generated by these treatments. To this end, splenic cDC1 and cDC2 from a B16-Flt3L tumor-bearing mice were used as DC source for the vaccine and tumor cell-lysate as tumor antigen. Vaccines were administered before or after challenging mice with tumors to assess their prophylactic or therapeutic anti-tumor efficacy and to explore the generated effector and memory immune response via flow cytometry. Furthermore, the effect of cDC1-based vaccination as a neoadjuvant or adjuvant treatment against tumor recurrence was explored using an experimental tumor relapse model. Flow cytometry and scRNAseq were mainly used to study immune responses. Finally, publicly available transcriptomic data from tumors of human patients were analyzed. The sample size per group, the number of independent experiments as well as the statistical methods are described in each figure legend.

Mice

Mouse colonies were bred at the CNIC under specific pathogen-free conditions. Wildtype mice were in C57BL/6 background and 6–10-week-old females were used for all experiments to limit complications of male territorial behavior and fighting during long-term cancer experiments. OT-I transgenic mice (C57BL/6-Tg (TcraTcrb)1100Mjb/J) and OT-II transgenic mice (C57BL/6-Tg (TcraTcrb)425Cbn), both crossed with B6-SJL (Ptprca Pepcb/BoyJ) mice expressing the CD45.1 allele were acquired from The Jackson Laboratory (Bar Harbor, ME, USA). $XCR1^{DTRvenus}$ mice[49] were kindly provided by Tsuneyasu Kaisho (Wakayama Medical University, Japan). Mice were group-housed, have not been used in previous procedures, and were fed standard chow diet. The ethical committee at CNIC and the Ethics Commitee/Animal Experimentation Subcommittee of the Universidad Autonoma de Madrid, as authorized body by the Comunidad de Madrid, evaluated the procedures and the Comunidad de Madrid approved all animal studies. Animal experiments followed protocols approved by the institutional ethics committee at the Centro Nacional de Investigaciones Cardiovasculares and conformed to EU Directive 86/609/EEC and Recommendation 2007/526/EC regarding the protection of animals used for experimental and other scientific purposes, enforced in Spanish law under Real Decreto 1201/2005. All mice were maintained on a 12-hour light/dark schedule in a specific pathogen-free animal facility in individually ventilated cages and were given food and water ad libitum. Ambient temperature in the animal facility was 20–24 °C, and relative humidity was 45–65%.

Cell culture and tumor models

B16-OVA (a kind gift from L. Chen, Yale University, New Haven, CT), MC38 (purchased from the ATCC/Kerafast accession ID: CVCL_B288), B16-Flt3L cells (kindly provided by G. Dranoff, Harvard University, Boston, MA) and B16-F10 (a kind gift from I. Malanchi, The Crick Institute, London, UK) were cultured at 37 °C in 5% CO_2 in R10 medium [RPMI Medium 1640 (Gibco®) with 10% heat-inactivated Fetal Bovine Serum (hi-FBS), 50 µM β-Mercaptoethanol (both Sigma), 2 mM L-Glutamine, 100 U/mL Penicillin and Streptomycin (100 µg both Lonza), 0.1 mM NEAA, 1 mM Sodium Pyruvate, 1 mM HEPES (all from HyClone™)]. All cell lines were tested for absence of mycoplasma using

the MycoAlert PLUS Mycoplasma Detection Kit (Lonza) according to manufacturer's instructions. Tumor cells were detached (5 mM EDTA/PBS) before reaching confluence 5×10^5 MC38 cells inoculated subcutaneous in 50 µl PBS into the shaved right flank of wildtype mice or 4×10^5 B16-OVA cells were inoculated intravenously unless otherwise specified in the experiment. For the colorectal carcinoma experimental relapse model, 5×10^5 MC38 cells were intradermally inoculated, tumors were surgically resected at day 10 and 30 days upon resection 1.5×10^6 MC38 cells were inoculated in the same flank, when the skin was completely healed. For the B16-F10 cancer relapse model, 10^5 B16-F10 cells were intradermally inoculated, tumors were surgically resected at day 12 and 7×10^5 B16-F10 cells were inoculated into the same flank 37 days after resection. Mice were treated with antibiotics (subcutaneous cefovecin, 25 µg/mice) right before surgery and analgesics (intraperitoneal buprenorphine, 3.6 µg/mice) before and the day after surgery. For antibody-depletion of $CD8^+$ and $CD4^+$ T cells, mice were intraperitoneally injected with 125 µg anti-CD8b (clone 53-5.8, BioXCell) or anti-CD4 (clone GK1.5, Biolegend) antibodies 3- and 1-day prior tumor re-challenge. Control mice were intraperitoneally injected with 125 µg IgG from rat serum (Sigma) on the same days. $CD4^+$ and $CD8^+$ T cell depletion in the blood was tested for every mouse. Tumor size was measured three times weekly using a digital caliper (Ratio), calculated as the product of orthogonal diameters and is displayed in mm^2. Tumors growing in the lung were quantified by counting lung nodules under a stereomicroscope or, when nodules were not clearly defined, by a quantifying the tumor-free and tumor-occupied lung area. Tumor-bearing mice were monitored daily and sacrificed to determine the survival curve when signs of adverse effects (pain, apathy, dehydration, necrotic tumor) were observed or the humane endpoint (tumor size diameter 1.7 cm) reached.

Tumor cell lysate preparation

TCL was generated as previously described[14]. Briefly, B16-OVA, B16-F10 or MC38 tumor cells were resuspended in R10 medium at 4×10^6 cells/ml, plated in a 6-well-plate, and treated with ~300 mJ/cm² UV irradiation using a Stratalinker UV Crosslinker 1800 (Stratagene). Cells were cultured for 16–24 h at 37 °C in 5% CO_2, subjected to 3 freeze (−80 °C) / thaw (37 °C) cycles of minimum 30 min each, and passed through a 40 µm cell strainer before addition to cDC1s or cDC2s at a ratio of 1 cDC to 2 tumor cells.

Tissue dissociation

Spleen, inguinal lymph nodes (iLNs), mediastinal lymph nodes (mdLN), auricular lymph nodes (auLN), and popliteal lymph nodes (pLN) were harvested in R10 medium. Spleen and LNs were digested for 10 min at 37 °C with 0.25 mg/ml Liberase TL (Roche) and 50 µg/ml DNaseI (Sigma Aldrich). Tumors, ears, and lungs were minced and incubated for 30 min in HBSS (Gibco®) shacking at 37 °C with 50 µg/ml DNaseI and 0.5 mg/ml Collagenase IV (Sigma) (tumors) or 0.25 mg/ml Liberase TL (Roche) (ears and lungs). Ears were passed through a 18 G syringe and squeezed through a 100 µm cell strainer (Corning). The rest of the tissues were squeezed through a 70 µm cell strainer (Corning). All tissues were re-filtered through a 40 µm cell strainer and spleen and lung subjected for 5 min to Red Blood Cell Lysis Buffer (Sigma).

Adoptive transfer of splenic cDCs and anti-PD1 treatment

For splenic cDC expansion, 2.5×10^6 B16-Flt3L cells were inoculated in 100 µl PBS subcutaneously into both flanks of C57BL/6 mice or tumor-free mice received a hydrodynamic injection of Flt3L-encoding plasmid (mFLEX), and spleens harvested 10-11 days thereafter. When cDC1s and cDC2s were used in the experiment (Figs. 1–4 and Supplementary Figs. 1–3), spleen single cell suspensions were subjected to positive selection of $CD11c^+$ cells using CD11c MicroBeads UltraPure (Miltenyi Biotec). Briefly, the single cell suspension was incubated for 15 minutes with CD11c MicroBeads in the presence of FcR block anti-mouse CD16/CD32 (2.4G2, Tonbo Biosciences), after which cells were purified using MACS® columns and stained with antibodies (as specified below). Then, Fluorescence-Activated Cell Sorting (FACS) was performed using a FACSAria II sorter (BD), in which cDC1s ($MHCII^+$ $CD11c^+$ $CD8^+$ $CD11b^-$) and cDC2s ($MHCII^+$ $CD11c^+$ $CD8^-$ $CD11b^+$) were collected. When only cDC1s were used in the experiment (Figs. 5, 6 and Supplementary Figs. 4–6), they were isolated using the mouse $CD8^+$ Dendritic Cell Isolation Kit using MACS® columns and autoMACS™ Running Buffer according to manufacturer's instructions (Miltenyi Biotec) as previously described[14]. Purified cDC1s and cDC2s were cultured in round-bottom 96-well plates (Corning) at 2×10^5 DCs/200 µl R10 medium for 1 h or 4 h, respectively (or as specified for experiments), at 37 °C in 5% CO_2 together with (as specified for experiments): 100 ng/ml LPS EK, 20 µg/ml poly I:C LMW, 5 µg/ml CpG ODN1826, 1 µg/ml R848 (all from InVivoGen) and/or B16-OVA, B16-F10 or MC38 TCL at a ratio of 1 DC to 2 tumor cells. DCs were washed with R10 and, when incubated with TCL, re-purified using MACS® columns. Cells were then administered intravenously (100 µl PBS, Gibco®) or intradermally (50 µl PBS) into mice, or co-cultured with OT-I or OT-II cells. Anti-PD-1 (clone RMP1–14 from BioXCell) was administered intraperitoneal at 100 µg/mouse in 100 µl PBS.

In vivo cDC migration assay and depletion of host cDC1s

Splenic cDC1s and cDC2s were FACS sorted from $CD45.2^+$ mice, cultured with B16-OVA TCL and CpG, and re-purified as previously indicated. Then, 10^6 cDC1s or cDC2s were adoptively transferred into the foot-pad of $CD45.1^+$ recipient mice via subcutaneous injection. The popliteal lymph node was harvested 20 h thereafter, processed, and the presence of $CD45.2^+$ cDC1s and cDC2s quantified by flow cytometry.

For depletion of endogenous cDC1s, $XCR1^{DTRvenus}$ mice were treated at the indicated time points with 25 ng/g DT (Sigma) intraperitoneally. The absence of host cDC1s was confirmed in mice treated simultaneously with experimental mice.

OT-I and OT-II cell proliferation and in vivo assays

For ex vivo proliferation assays, splenic naive $CD8^+$ OT-I and $CD4^+$ OT-II cells were purified from CD45.1 OT-I and CD45.1 OT-II transgenic mice via FACS sorting of $CD8^+$ or $CD4^+$ cells, respectively, that were $CD62L^+$ and $CD44^-$. Cells were then labeled with CellTrace™ Violet Cell Proliferation Kit (Thermofisher, Molecular Probes) according to manufacturer's instructions. cDC1s or cDC2s were FACS sorted from pre-purified $CD11c^+$ cells from the spleen of untreated or B16-Flt3L bearing mice, and cultured for 1, 4, or 16 hours in the presence of B16-OVA TCL (1 cDC to 2 tumor cells ratio)] and/or a combination of adjuvants (100 ng/ml LPS EK, 20 µg/ml poly I:C LMW, 5 µg/ml CpG ODN1826, 1 µg/ml R848] as specified in the experiment. cDCs were then re-purified using MACS® columns and co-cultured with 10^4 labeled OT-I or OT-II cells in a 1:1 ratio. After 4-5 days of co-culture (OT-I and OT-II, respectively), T cell proliferation was assessed by flow cytometry by dilution of the CellTrace™ Violet dye.

For in vivo assays, naive OT-I cells were purified using the EasySepTM Mouse Naive $CD8^+$ T Cell Isolation kit (Stemcell Technology), following the manufacturer's instructions. $2–3 \times 10^5$ OT-I cells were injected in 100 µl PBS intravenously in mice. One day thereafter, cDC1s or cDC2s were injected and mice analyzed as described for the individual experiments.

Fluorescent staining, flow cytometry, and cell sorting

Single cell suspensions of cDC1s, cDC2, spleen, iLN, mdLN, auLN, pLN, blood, ear skin and tumors or cultured OT-I or OT-II cells were incubated for 20 min at 4 °C in PBS with 2% FBS and 0.5 mM EDTA (Sigma) with FcR block anti-mouse CD16/CD32 (clone 2.4G2, Tonbo Biosciences) and a mix of the following fluorochrome-conjugated antibodies: anti-mouse CD45.1 (clone A20), CD45 (clone 30-F11), CD44

(clone IM7), SIRPα (clone P84), DC-SIGN (CD209, clone 22D1), F4/80 (clone BM8) and CD62L (clone MEL-14) from eBioscience™, CD8 (clone 53–6.7), CD11b (clone M1/70), SiglecF (clone E50-2440), CD69 (clone H1.2F3), B220 (clone RA3-6B2), Ly6G (clone 1A8), F4/80 (cone T45-2342), CD64 (X54-5/7.1) and I-A/I-E (MHC-II, clone 2G9) from BD Biosciences, CD3 (clone 17A2) from Tonbo Biosciences, MERTK (clone DS5MMER) and Ly6C (clone HK1.4) from Invitrogen and CD11c (clone N418), XCR1 (clone ZET), CD103 (clone 2E7), CCR2 (clone SA2036H), CD115 (clone AF598), CD24 (clone M1/69), CXCR6 (clone SA051D1) and CD90 (clone 53-2.1) from BioLegend. All antibodies were used 1:200, except anti-I-A/I-E antibody, which was used 1:400. DAPI (Sigma) was used to exclude dead cells. The LSRFortessa cell analyzer and FACSAria Cell Sorter (BD Biosciences) were used. FACSDiva software (BD Biosciences) and FlowJo Version 10 were used to record and analyze data.

T cell re-stimulation assays

Antigen re-stimulation assays using IFNγ, TNFα, or IL17A staining as readout were used to identify tumor specific T cells. Briefly, single cell suspensions of lymph nodes were re-stimulated ex vivo with antigen-loaded APCs (details see below) or OVA protein (20 µg/ml, Sigma Aldrich) plus MHC class II $OVA_{323–339}$ peptide (5 µM, GenScript) for 2 h in R10 at 37 °C in 5% CO_2 followed by 5 µg/mL Brefeldin A (Sigma Aldrich) treatment for 4 h. Cells were then labeled with the indicated surface-staining antibodies, fixed with 4% PFA (Thermofisher), permeabilized with 1% Bovine Serum Albumin, 0.1% Saponin, 0.02% Sodium Azide (all Sigma) in PBS and stained with anti-mouse IFNγ antibody (clone XMG1.2), TNFα (clone MP6-XT22) or IL17A (clone TC11-18H10.1) from BioLegend. APCs were generated from bone marrow cells that were harvested by flushing the tibia and femur. After red blood cell lysis, cells were cultured in R10 with 20 ng/ml murine GM-CSF (Peprotech) for 7 days. Floating cells were harvested and incubated with B16-OVA TCL, MC38 TCL, MHC class I $OVA_{257–264}$ peptide (GenScript), or MHC class II $OVA_{323–339}$ peptide for 8 h followed by addition of 100 ng/ml LPS-EK (InvivoGen) for another 12 h.

RNA purification and qRT-PCR

Total RNA was extracted with the RNeasy Micro Kit (Qiagen) and reverse transcribed using the High Capacity cDNA Reverse Transcription Kit with random hexamers (Applied Biosystems®) following manufacturer's instructions. Quantitative PCR was performed using the GoTaq® qPCR Master Mix (Promega) in a 7900HT Fast Real-Time PCR System (Applied Byosystem®). $2^{-\Delta Ct}$ mRNA expression values of mouse *Ifnb1*, *Il12b*, *Cd40* and *Ccr7* were calculated relative to expression of *18S rRNA*. The following primers (Sigma) were used:

18S rRNA-sense (5′)– GTAACCCGTTGAACCCCATT–(3′),
18S rRNA-antisense (5′)– CCATCCAATCGGTAGTAGCG–(3′);
Ifnb1-sense (5′)–TCAGAATGAGTGGTGGTTGC–(3′),
Ifnb1-antisense (5′)–GACCTTTCAAATGCAGTAGATTCA–(3′);
Il12b-sense (5′)–GGAAGCACGGCAGCAGAATA–(3′),
Il12b-antisense (5′)–AACTTGAGGGAGAAGTAGGAATGG–(3′);
Cd40-sense (5′)–TTGTTGACAGCGGTCCATCTA–(3′),
Cd40-antisense (5′)–GCCATCGTGGAGGTACTGTTT–(3′);
Ccr7-sense (5′)–TGTACGAGTCGGTGTGCTTC–(3′),
Ccr7-antisense (5′)–GGTAGGTATCCGTCATGGTCTTG–(3′).

scRNAseq

For single cell analysis of tumor infiltrating lymphocytes (TILs), tumors were processed to obtain single-cell suspensions. Cells from each biological replicate (6 per experimental group) were pooled in equal cell numbers in $n = 2$ per experimental condition and independently labeled using Cell Multiplexing Oligos (CMOs, 10x Genomics), following the manufacturer's protocol. Cells were then antibody-stained and DAPI$^-$CD45$^+$CD3$^+$CD90$^+$ cells that were CD8$^+$ or CD4$^+$ were FACS sorted and equal numbers of cells per replicate were mixed. Finally, the mixed cell suspension was processed using the 10x Genomics 3′ v2 kit, as specified by the manufacturer's instructions. Libraries were sequenced on the Illumina HiSeq 4000 platform using 100 bp paired-end reads.

Single-cell RNA-sequencing data were processed using the Cell Ranger (v6.1.2) default parameters and the mm10 (GRCm38.p6) mouse genome reference provided by 10x Genomics. Results from RNA quantification were imported into R (v4.1.2) and analyzed using Seurat (v4.2.1)[80]. Cells were filtered to retain those with <10% mitochondrial RNA content, more than 300 genes, and with a number of unique molecular identifiers (UMIs) comprised between 500 and 50,000. Then, the remaining cells were demultiplexed using the cellhashR R package (v1.0.2[81]) using htodemux, bff_cluster, gmm_demux, multiseq, and dropletutils methods. The consensus classification was finally used for further analyses. In addition, contamination of cells not expressing CD3 or CD90 were excluded, resulting in a total of 15,253 analyzed cells. Next, counts were normalized for library size using Seurat's default normalization parameters. RNA count was used as a source of unwanted variation and regressed using Seurat's built-in regression model. Highly variable genes were identified using Seurat, which were used to perform principal component analysis. The first 20 principal components were used as an input for clustering using Louvain algorithm and for visualization using the t-Distributed Stochastic Neighbor Embedding (t-SNE) algorithm using default parameters. Marker genes for each cluster were identified using the Wilcoxon rank sum test implemented in Seurat. Moreover, marker genes were required to be expressed by at least 25% of the cells in the cluster at a minimum fold change of 0.25. A total of 13 cell clusters were identified, which were manually annotated according to the expression of key markers and general genes characteristic for T cells. The calculation of differentially expressed genes between cells in different clusters was done using the FindMarkers function in Seurat using the Wilcoxon rank sum test and the gene set (pathway) enrichment analysis performed using the FGSEA algorithm, with genes ranked by logFC and KEGG database (KEGGREST package v1.46.0). The relative distribution of cells from different experimental conditions among clusters, together with the frequency of the sorted cells within all tumor cells, was used to calculate the total frequency of each cluster within tumors for every experimental condition.

Analysis of cancer patient data

This paper analyzes existing, publicly available data generated by the TCGA Research Network: https://www.cancer.gov/tcga and from GSE176078[59]. All normal tissue samples were removed from the analysis. Normalized log2 transformed expression matrixes were used to calculate cell signature scores per sample using MCP-counter R package (v1.2.0)[82]. The cDC1 signature[32] (*CLNK*, *BATF3*, *XCR1*, and *CLEC9A*), the human BRCA CD4$^+$ Trm signature (genes significantly upregulated in the CD4$^+$ Trm cluster[54] as compared with the other clusters FDR adj. p value ≤ 0.01 and log fold change ≥ 1.0) and the cDC1-induced CD4$^+$ Trm signature in mice (genes significantly upregulated in the CD4$^+$ Trm cluster from the scRNAseq data generated in the present study as compared with the other clusters, log fold change ≥ 1.0 and adj. p value ≤ 0.05) were used (Table S1). Correlation analyses were done using R.

Data from GSE176078[59] from 26 BRCA patients were used for further single-cell RNAseq analysis. Briefly, originally annotated CD4$^+$ T cells were re-integrated based on patient of origin using Seurat (functions FindIntegrationAnchors (using Canonical Correlation Analysis) and IntegrateData (both using the SCT normalization method)). Patients with less than 100 CD4$^+$ T cells (4 out of 26) could not be successfully integrated and were removed from the analysis. Features used for integration were then used to perform a principal component analysis. The first 20 principal components were used as input for clustering and embedding using the Uniform Manifold Approximation Projection (UMAP). A total of 17 clusters were identified. The frequency of the CD4$^+$ Trm (Cluster 16) and the cDC1:CLEC9A[59] cluster within all

tumor cells was calculated and used to perform Pearson's correlation analysis using R. Alternatively, the presence of cDC1 and $CD4^+$ Trm were deconvoluted from BRCA samples from the TCGA using the digitalDLsorteR R package (v1.1.2) as detailed elsewhere[60] and using default parameters. For survival analysis, patients without overall survival data and male patients with BRCA were removed. Mantel-Cox test was assessed in R, using the survdiff function (survival package v3.7) and represented using the package ggsurvfit (v1.1). Hazard-Ratios and 95% coefficient intervals were represented with R.

Statistical analysis

Data analysis employed GraphPad Prism version 8.0 and R for RNA sequencing analyses and patient survival analysis (see details above). Data are presented as mean ± standard error of the mean (SEM) and were analyzed, as indicated in the Figure legends, using one-way ANOVA and Tukey post hoc test, Mantel-Cox test, and two-way ANOVA. When indicated, log-transformed values are represented and used for statistical analysis. All experiments, except the confirmatory T cell memory induction experiment in Fig. 4d-g (performed once with n = 3–4/group), the confirmatory B16-F10 cancer relapse experiment in Fig. 5g–i (performed once with n = 6–7/group) and the scRNAseq in Fig. 6 (n = 2), were repeated at least twice, and either representative experiments or pooled data from several experiments are shown as indicated in the figure legends. Mice were allocated randomly in different experimental groups, but no specific randomization test was used. Researchers were generally blinded to group allocation when doing and analyzing experiments. All n values represent biological replicates (different mice, primary cell preparations, or in vitro experiments).

Reporting summary

Further information on research design is available in the Nature Portfolio Reporting Summary linked to this article.

Data availability

The scRNAseq data generated in this study have been deposited in GEO under the accession code GSE249585. The scRNAseq data of human BRCA patients are available in the GEO database under the accession code GSE176078. TCGA gene expression data for skin cutaneous melanoma (SKCM) and breast carcinoma (BRCA) are available in the Broad Institute Firehose portal (https://gdac.broadinstitute.org/) and summarized pan-cancer clinical data are available in the synapse database under the accession code syn12026747. Source data are provided with this paper.

Code availability

Code used for transcriptomic analysis has been deposited at GitHub https://github.com/DSanchoLab/Heras-Murillo_cDC1vaccine_2024.

References

1. Robert, C. A decade of immune-checkpoint inhibitors in cancer therapy. *Nat. Commun.* **11**, 3801 (2020).
2. Sharma, P., Hu-Lieskovan, S., Wargo, J. A. & Ribas, A. Primary, adaptive, and acquired resistance to cancer immunotherapy. *Cell* **168**, 707–723 (2017).
3. Dillekås, H., Rogers, M. S. & Straume, O. Are 90% of deaths from cancer caused by metastases? *Cancer Med.* **8**, 5574–5576 (2019).
4. Correia, A. L. Locally sourced: site-specific immune barriers to metastasis. *Nat. Rev. Immunol.* https://doi.org/10.1038/s41577-023-00836-2 (2023).
5. Jameson, S. C. & Masopust, D. Understanding subset diversity in T cell memory. *Immunity* **48**, 214–226 (2018).
6. Jin, Y. et al. Prognostic impact of memory CD8(+) T cells on immunotherapy in human cancers: a systematic review and meta-analysis. *Front. Oncol.* **11**, 698076 (2021).
7. Pagès, F. et al. Effector memory T cells, early metastasis, and survival in colorectal cancer. *N. Engl. J. Med.* **353**, 2654–2666 (2005).
8. Tay, R. E., Richardson, E. K. & Toh, H. C. Revisiting the role of CD4+ T cells in cancer immunotherapy—new insights into old paradigms. *Cancer Gene Ther.* **28**, 5–17 (2021).
9. Wu, J. et al. Tumor-infiltrating CD4+ central memory T cells correlated with favorable prognosis in oral squamous cell carcinoma. *JIR* **ume 15**, 141–152 (2022).
10. Zhang, H., Zhu, Z., Modrak, S. & Little, A. Tissue-resident memory CD4+ T cells play a dominant role in the initiation of antitumor immunity. *J. Immunol.* **208**, 2837–2846 (2022).
11. Nizard, M. et al. Induction of resident memory T cells enhances the efficacy of cancer vaccine. *Nat. Commun.* **8**, 15221 (2017).
12. Park, S. L. et al. Tissue-resident memory CD8+ T cells promote melanoma–immune equilibrium in skin. *Nature* **565**, 366–371 (2019).
13. Enamorado, M. et al. Enhanced anti-tumour immunity requires the interplay between resident and circulating memory CD8+ T cells. *Nat. Commun.* **8**, 1–11 (2017).
14. Wculek, S. K. et al. Effective cancer immunotherapy by natural mouse conventional type-1 dendritic cells bearing dead tumor antigen. *J Immunother Cancer.* **5**, 1–16 (2019).
15. Badovinac, V. P., Messingham, K. A. N., Jabbari, A., Haring, J. S. & Harty, J. T. Accelerated CD8+ T-cell memory and prime-boost response after dendritic-cell vaccination. *Nat. Med.* **11**, 748–756 (2005).
16. Vreeland, T. J. et al. A phase IIb randomized controlled trial of the TLPLDC vaccine as adjuvant therapy after surgical resection of stage III/IV melanoma: a primary analysis. *Ann. Surg. Oncol.* **28**, 6126–6137 (2021).
17. Bloemendal, M. et al. Immunological responses to adjuvant vaccination with combined CD1c+ myeloid and plasmacytoid dendritic cells in stage III melanoma patients. *OncoImmunology* **11**, 1–12 (2022).
18. Cabeza-Cabrerizo, M., Cardoso, A., Minutti, C. M., Pereira Da Costa, M. & Reis E Sousa, C. Dendritic cells revisited. *Annu. Rev. Immunol.* **39**, 131–166 (2021).
19. Burch, P. A. et al. Priming tissue-specific cellular immunity in a phase I trial of autologous dendritic cells for prostate cancer. *Clin. Cancer Res.* **6**, 2175–2182 (2000).
20. Carreno, B. M. et al. A dendritic cell vaccine increases the breadth and diversity of melanoma neoantigen-specific T cells. *Science* **348**, 803–808 (2015).
21. Kleindienst, P. & Brocker, T. Endogenous dendritic cells are required for amplification of T cell responses induced by dendritic cell vaccines in vivo. *J. Immunol.* **170**, 2817–2823 (2003).
22. Yewdall, A. W., Drutman, S. B., Jinwala, F., Bahjat, K. S. & Bhardwaj, N. CD8+ T cell priming by dendritic cell vaccines requires antigen transfer to endogenous antigen presenting cells. *PLoS ONE* **5**, e11144 (2010).
23. Ashour, D. E. D. et al. IL-12 from endogenous cDC1, and not vaccine DC, is required for Th1 induction. *JCI Insight* **5**, e135143 (2020).
24. Ferris, S. T. et al. cDC1 vaccines drive tumor rejection by direct presentation independently of host cDC1. *Cancer Immunol. Res.* **10**, 920–931 (2022).
25. Den Haan, J. M. M., Lehar, S. M. & Bevan, M. J. CD8+ but not CD8- dendritic cells cross-prime cytotoxic T cells in vivo. *J. Exp. Med.* **192**, 1685–1695 (2000).
26. Bachem, A. et al. Superior antigen cross-presentation and XCR1 expression define human CD11c+CD141+ cells as homologues of mouse CD8+ dendritic cells. *J. Exp. Med.* **207**, 1273–1281 (2010).
27. Ferris, S. T. et al. cDC1 prime and are licensed by CD4+ T cells to induce anti-tumour immunity. *Nature* **584**, 624–629 (2020).
28. Sánchez-Paulete, A. R. et al. Cancer immunotherapy with immunomodulatory anti-CD137 and anti–PD-1 monoclonal antibodies

requires BATF3-dependent dendritic cells. *Cancer Discov.* **6**, 71–79 (2016).
29. Teijeira, A. et al. Depletion of conventional type-1 dendritic cells in established tumors suppresses immunotherapy efficacy. *Cancer Res.* https://doi.org/10.1158/0008-5472.can-22-1046 (2022).
30. Salmon, H. et al. Expansion and activation of CD103+ dendritic cell progenitors at the tumor site enhances tumor responses to therapeutic PD-L1 and BRAF inhibition. *Immunity* **44**, 924–938 (2016).
31. Hubert, M. et al. IFN-III is selectively produced by cDC1 and predicts good clinical outcome in breast cancer. *Sci. Immunol.* **5**, 1–16 (2020).
32. Böttcher, J. P. et al. NK cells stimulate recruitment of cDC1 into the tumor microenvironment promoting cancer immune control. *Cell* **0**, 1–16 (2018).
33. Zhou, Y. et al. Vaccine efficacy against primary and metastatic cancer with in vitro-generated CD103 + conventional dendritic cells. *J. Immunother. Cancer* **8**, 1–13 (2020).
34. Schwarze, J. K. et al. Intratumoral administration of CD1c (BDCA-1) $^{+}$ and CD141 (BDCA-3) $^{+}$ myeloid dendritic cells in combination with talimogene laherparepvec in immune checkpoint blockade refractory advanced melanoma patients: a phase I clinical trial. *J. Immunother. Cancer* **10**, e005141 (2022).
35. Binnewies, M. et al. Unleashing type-2 dendritic cells to drive protective antitumor CD4+ T cell immunity. *Cell* **177**, 556–571.e16 (2019).
36. Tel, J. et al. Human plasmacytoid dendritic cells efficiently cross-present exogenous Ags to CD8+ T cells despite lower Ag uptake than myeloid dendritic cell subsets. *Blood* **121**, 459–467 (2013).
37. Segura, E. et al. Characterization of resident and migratory dendritic cells in human lymph nodes. *J. Exp. Med.* **209**, 653–660 (2012).
38. Duong, E. et al. Type I interferon activates MHC class I-dressed CD11b+ conventional dendritic cells to promote protective anti-tumor CD8+ T cell immunity. *Immunity* **55**, 308–323.e9 (2022).
39. Ruhland, M. K. et al. Visualizing synaptic transfer of tumor antigens among dendritic cells. *Cancer Cell* **37**, 786–799.e5 (2020).
40. Westdorp, H. et al. Blood-derived dendritic cell vaccinations induce immune responses that correlate with clinical outcome in patients with chemo-naive castration-resistant prostate cancer. *J. Immunother. Cancer* **7**, 1–15 (2019).
41. Bol, K. F. et al. The clinical application of cancer immunotherapy based on naturally circulating dendritic cells. *J. Immunother. Cancer* **7**, 1–13 (2019).
42. Bol, K. F. et al. Adjuvant dendritic cell therapy in stage IIIB/C melanoma: the MIND-DC randomized phase III trial. *Nat. Commun.* **15**, 1632 (2024).
43. Laoui, D. et al. The tumour microenvironment harbours ontogenically distinct dendritic cell populations with opposing effects on tumour immunity. *Nat. Commun.* **7**, 1–17 (2016).
44. Wculek, S. K. et al. Dendritic cells in cancer immunology and immunotherapy. *Nat. Rev. Immunol.* **20**, 7–24 (2020).
45. Poulin, L. F. et al. Characterization of human DNGR-1 $^{+}$ BDCA3 $^{+}$ leukocytes as putative equivalents of mouse CD8α $^{+}$ dendritic cells. *J. Exp. Med.* **207**, 1261–1271 (2010).
46. Brown, C. C. et al. Transcriptional basis of mouse and human dendritic cell heterogeneity article transcriptional basis of mouse and human dendritic cell heterogeneity. 846–863 https://doi.org/10.1016/j.cell.2019.09.035.
47. Cueto, F. J. & Sancho, D. The Flt3L/Flt3 axis in dendritic cell biology and cancer immunotherapy. *Cancers* **13**, 1525 (2021).
48. Pantel, A. et al. Direct type I IFN but not MDA5/TLR3 activation of dendritic cells is required for maturation and metabolic shift to glycolysis after poly IC stimulation. *PLoS Biol.* **12**, e1001759 (2014).
49. Yamazaki, C. et al. Critical roles of a dendritic cell subset expressing a chemokine receptor, XCR1. *J. Immunol.* **190**, 6071–6082 (2013).
50. Curti, B. D. & Faries, M. B. Recent advances in the treatment of melanoma. *N. Engl. J. Med.* **384**, 2229–2240 (2021).
51. Tay, C., Tanaka, A. & Sakaguchi, S. Tumor-infiltrating regulatory T cells as targets of cancer immunotherapy. *Cancer Cell* **41**, 450–465 (2023).
52. Oliveira, G. et al. Landscape of helper and regulatory antitumour CD4+ T cells in melanoma. *Nature* **605**, 532–538 (2022).
53. Zhang, L. et al. Single-cell analyses inform mechanisms of myeloid-targeted therapies in colon cancer. *Cell* **181**, 442–459.e29 (2020).
54. Savas, P. et al. Single-cell profiling of breast cancer T cells reveals a tissue-resident memory subset associated with improved prognosis. *Nat. Med.* **24**, 986–993 (2018).
55. Mueller, S. N. & Mackay, L. K. Tissue-resident memory T cells: Local specialists in immune defence. *Nat. Rev. Immunol.* **16**, 79–89 (2016).
56. Ali, H. R. et al. Association between CD8+ T-cell infiltration and breast cancer survival in 12 439 patients. *Ann. Oncol.* **25**, 1536–1543 (2014).
57. Leader, A. M. et al. Single-cell analysis of human non-small cell lung cancer lesions refines tumor classification and patient stratification. *Cancer Cell* **39**, 1594–1609.e12 (2021).
58. The Cancer Genome Atlas Research Network. et al. The Cancer Genome Atlas Pan-Cancer analysis project. *Nat. Genet* **45**, 1113–1120 (2013).
59. Wu, S. Z. et al. A single-cell and spatially resolved atlas of human breast cancers. *Nat. Genet.* **53**, 1334–1347 (2021).
60. Torroja, C. & Sanchez-Cabo, F. Digitaldlsorter: Deep-Learning on scRNA-Seq to Deconvolute Gene Expression Data. *Front Genet* **10**, 978 (2019).
61. Heras-Murillo, I., Adán-Barrientos, I., Galán, M., Wculek, S. K. & Sancho, D. Dendritic cells as orchestrators of anticancer immunity and immunotherapy. *Nat. Rev. Clin. Oncol.* https://doi.org/10.1038/s41571-024-00859-1 (2024).
62. Naik, S. H. et al. Cutting edge: generation of splenic CD8+ and CD8- dendritic cell equivalents in Fms-like tyrosine kinase 3 ligand bone marrow cultures. *J. Immunol.* **174**, 6592–6597 (2005).
63. Iyoda, T. et al. The CD8+ dendritic cell subset selectively endocytoses dying cells in culture and in vivo. *J. Exp. Med.* **195**, 1289–1302 (2002).
64. Liu, J. et al. Improved efficacy of neoadjuvant compared to adjuvant immunotherapy to eradicate metastatic disease. *Cancer Discov.* **6**, 1382–1399 (2016).
65. Mittendorf, E. A., Burgers, F., Haanen, J. & Cascone, T. Neoadjuvant Immunotherapy: Leveraging the Immune System to Treat Early-Stage Disease. *American Society of Clinical Oncology Educational Book* 189–203 (2022).
66. Grossmann, K. F. et al. Adjuvant pembrolizumab versus IFNα2b or ipilimumab in resected high-risk melanoma. *Cancer Discov.* **12**, 644–653 (2022).
67. Garg, A. D., Coulie, P. G., Van den Eynde, B. J. & Agostinis, P. Integrating next-generation dendritic cell vaccines into the current cancer immunotherapy landscape. *Trends Immunol.* **38**, 577–593 (2017).
68. Ahn, E. et al. Role of PD-1 during effector CD8 T cell differentiation. *Proc. Natl. Acad. Sci. USA* **115**, 4749–4754 (2018).
69. Djenidi, F. et al. CD8+CD103+ tumor–infiltrating lymphocytes are tumor-specific tissue-resident memory T cells and a prognostic factor for survival in lung cancer patients. *J. Immunol.* **194**, 3475–3486 (2015).
70. Luoma, A. M. et al. Tissue-resident memory and circulating T cells are early responders to pre-surgical cancer immunotherapy. *Cell* **185**, 2918–2935.e29 (2022).
71. Cañellas-Socias, A. et al. Metastatic recurrence in colorectal cancer arises from residual EMP1+ cells. *Nature* **611**, 603–613 (2022).

72. Lei, X. et al. CD4+ helper T cells endow cDC1 with cancer-impeding functions in the human tumor micro-environment. *Nat. Commun.* **14**, 217 (2023).
73. Espinosa-Carrasco, G. et al. Intratumoral immune triads are required for immunotherapy-mediated elimination of solid tumors. *Cancer Cell* **42**, 1202–1216.e8 (2024).
74. Magen, A. et al. Intratumoral dendritic cell-CD4+ T helper cell niches enable CD8+ T cell differentiation following PD-1 blockade in hepatocellular carcinoma. *Nat. Med.* **29**, 1389–1399 (2023).
75. Beura, L. K. et al. CD4+ resident memory T cells dominate immunosurveillance and orchestrate local recall responses. *J. Exp. Med.* **216**, 1214–1229 (2019).
76. Wu, T. D. et al. Peripheral T cell expansion predicts tumour infiltration and clinical response. *Nature* **579**, 274–278 (2020).
77. Cohen, M. et al. The interaction of CD4+ helper T cells with dendritic cells shapes the tumor microenvironment and immune checkpoint blockade response. *Nat. Cancer* **3**, 303–317 (2022).
78. Zhang, L. et al. Lineage tracking reveals dynamic relationships of T cells in colorectal cancer. *Nature* **564**, 268–272 (2018).
79. Aarntzen, E. H. J. G. et al. Targeting CD4+ T-helper cells improves the induction of antitumor responses in dendritic cell -based vaccination. *Cancer Res.* **73**, 19–29 (2013).
80. Butler, A., Hoffman, P., Smibert, P., Papalexi, E. & Satija, R. Integrating single-cell transcriptomic data across different conditions, technologies, and species. *Nat. Biotechnol.* **36**, 411–420 (2018).
81. Boggy, G. J. et al. BFF and cellhashR: analysis tools for accurate demultiplexing of cell hashing data. *Bioinformatics* **38**, 2791–2801 (2022).
82. Becht, E. et al. Estimating the population abundance of tissue-infiltrating immune and stromal cell populations using gene expression. *Genome Biol.* **17**, 1–20 (2016).

Acknowledgements

We thank the members of the D.S. laboratory and the laboratory of Salvador Iborra for discussions and critical reading of the manuscript. We thank the staff at the CNIC technical units; especially the Animal, Cellomics, and Genomics facilities for technical support. This project was supported by the "la Caixa" Foundation (ID 100010434) INPhINIT Fellowship code LCF/BQ/IN17/11620074 (IHM). IM lab work was supported by Fundación Fero. The SKW laboratory and this work is supported by the IRB Barcelona, the European Union and European Research Council's Horizon Europe programme (ERC-2023-StG 'MyTissue' project number 101117470); by grants RYC2022-036400-I and PID2022-140715OA-I00 from MCIN/AEI/10.13039/501100011033 Agencia Estatal de Investigación, Unión Europea NextGenerationEU/PRTR. IRB Barcelona receives institutional funding from the Spanish Ministry of Science and Innovation through the Centres of Excellence Severo Ochoa Award and from the CERCA Programme / Generalitat de Catalunya. Work in the DS laboratory is funded by the CNIC; by Ministerio de Ciencia, Innovación y Universidades (MICIU) PID2022-137712OB-I00, CPP2021-008310 and CPP2022-009762 MICIU/AEI/10.13039/501100011033 Agencia Estatal de Investigación, Unión Europea NextGenerationEU/PRTR; by Comunidad de Madrid (P2022/BMD-7333 INMUNOVAR-CM); by Scientific Foundation of the Spanish Association Against Cancer (AECC- PRYGN246642SANC); by Worldwide Cancer Research 25-0080; by European Union ERC-2023-PoC; by a research agreement with Inmunotek S.L.; and by "la Caixa" Foundation (LCF/PR/HR23/52430012 and LCF/PR/HR22/52420019). This study was also supported by "la Caixa" Foundation (LCF/PR/HR20/00075 to D.S. and M.A.P.). PID2020-118658RB-I00 (MCIN/AEI/10.13039/501100011033), and PROYE20089DELP (Asociación Española Contra el Cáncer, AECC) to MAP. The CNIC is supported by the Instituto de Salud Carlos III (ISCIII), the MICIU, and the Pro CNIC Foundation, and is a Severo Ochoa Center of Excellence (CEX2020-001041-S funded by MICIU/AEI /10.13039/501100011033).

Author contributions

I.H.M., S.K.W., and D.S. conceptualized the study, designed the experiments, and wrote the manuscript. I.H.M., P.M., V.N., J.H., and S.K.W. performed experiments and analyzed most of the data. I.H.M. and D.M. carried out the bioinformatics analysis. M.C.M. and M.A. helped with mouse tumor models supervised by M.A.P. and I.M. respectively, who also provided strategic advice. S.K.W. and D.S. funded and supervised the research.

Competing interests

S.K.W. serves as a consultant for ONA therapeutics (Barcelona, Spain). D.S. has a research collaboration agreement with Inmunotek SL (Alcala de Henares). I.M. reports grant funding from Roche, BMS, Astrazeneca, Genmab, and Pharmamar and advisory roles with Roche-Genentech, Bristol-Myers Squibb, Astrazeneca, F-Star, Genmab, Third Rock Ventures, Amunix Pharmaceuticals, Alligator, Bioncotech, Boston Therapeutics, Bright Peak, Numab, Catalym, Pieris, and Pharmamar. The rest of the authors declare no competing interests.

Additional information

Supplementary information The online version contains supplementary material available at https://doi.org/10.1038/s41467-025-58289-1.

Correspondence and requests for materials should be addressed to Stefanie K. Wculek or David Sancho.

Peer review information *Nature Communications* thanks Damya Laoui, Pawel Kalinski, and Michele De Palma for their contribution to the peer review of this work. A peer review file is available.